FACILE FABRICATION OF CHALCOGENIDE NANOPARTICLES

YASSIN MOHAMED

A thesis submitted in partial fulfilment of the requirements of the Manchester Metropolitan University for the degree of Master of Research

School of Science and the Environment

Division of Chemistry and Environmental Science

the Manchester Metropolitan University

June 2013

Acknowledgments

In the name of God, the most merciful, the most beneficent

Firstly, without the will of God I would not have had the chance to embark on this challenge. I would not have had the chance to research the information presented here. I would like to thank Dr. Craig Banks for giving me the opportunity of a lifetime to undertake this Masters Degree, who has been nothing but supportive in my research and has helped me every step of the way. Also, I would like to thank Dr. Dimitrios Kampourious for his constant guidance on this journey. Thank you to my father Ahmed Ibrahim and mother Faisa Xaji Ali, for the financial and moral support to keep me going in the darkest times. They truly are my inspiration. Thanks also need to go to Dr. Chris Rego and the Craig Banks research group. Finally, a big thank you to my family and friends for supporting me and being there for me when I needed help.

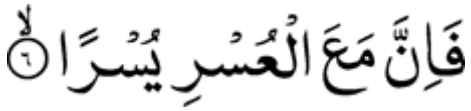

Verily, after hardship comes ease (Al Sharh)

Abstract

Nanotechnology is expected to be the basis of many of the main technological innovations of the twenty first century. Research and development in this field is growing rapidly throughout the world. A major output of this activity is the development of new materials in the nanometre scale. In this thesis, primarily, a novel fabrication of metal chalcogenides in the nano region is presented. The synthetic route is possible in less than 2 minutes in an aqueous based system using mercury nitrate and a sulfide precursor; which has a rate of reaction almost tenfold quicker than previous literature. To stabilise the compound, a range of surfactants and solvents were used in order to form monodispersed colloidal chalcogenide solutions. Using this approach, it is shown for the first time that metal chalcogenides can be solution-stabilised for greater than 2 minutes using Nafion®.

This thesis highlights the ways in which the newly found method of synthesis for metal chalcogenides can be extended onto a range of salts such as cadmium sulfide and bismuth sulfide. Nafion was also extended and implemented in stabilising these salts to show that the method is extendable to a wide range of solutions. This has so far eradicated the problem of coalescing in group II- VI semiconductors maintaining their 1:1 ratio (metal: precursor) ultimately maintaining their unique properties which is the basis behind their roles. Finally, the attachment of siRNA onto a well-known nanostructure was explored.

Contents

1. Introduction to Nanotechnology

1.1 History

The nanoscale range is defined as being between 0.2 nm (the atomic level) and around 100 nm [1]. This is the range that substantial differences are noticed as opposed to the same substance at greater sizes.[1] This is due to the larger surface area to mass ratio and quantum effects which start to come into effect at these dimensions, which ultimately leads to significant changes in several types of the nanoparticles (NPs) physical properties [1]. Current knowledge of science at the nanometre scale is derived from many disciplines, originating with the atomic and molecular concepts in chemistry and physics, and then incorporating molecular life sciences, medicine and engineering [1].

The NPs have an exceptionally high surface area to volume ratio; this is one of the reasons for some of their unusual properties. Scientific areas such as electronic, electro-optic and optical devices are some of the fields which nanoscience is significantly impacting [2].

Nanotechnology is dependent on nanostructures that require synthesis and characterisation. The properties of NPs differ remarkably both physically and chemically in terms of morphology, surface area, surface charge, purity and the media in which they are present. In addition, they differ in regards to degree of aggregation in a particular system which will strongly influence the bioavailability, mobility and transformation [3].

Two fundamentally different approaches for the controlled generation of nanostructures have evolved. On one hand there is growth and self-assembly, from the *bottom up,* involving

single atoms and molecules [1]. On the other hand is *top down* synthesis which usually involves large uniform pieces of material and generate the required nanostructures [2]. An example of this can be attrition/ milling. Currently, the favourable approach remains top down assembly methodologies, as the nanostructures can be synthesised on both small and large scale. A well-known method includes molecular beam epitaxy (MBE). This has its disadvantages which include time taken to synthesise and running expenses. Problems have been noted with this approach as a whole such as reproducibility and safety [1]. It is reported that bottom-up assembly is very powerful in creating identical structures with atomic precision.

Nanoparticles are best known for their shape and size [4]. Nanoparticles can be presented as an aerosol (mostly solid or liquid phase in air), a suspension (mostly solid in liquids) or as an emulsion (two liquid phases).

1.2 Fundamentals of Nucleation

The fundamentals behind the nucleation of nanoparticles are based on simple and inter-changeable factors. A solution with solute exceeding the solubility or supersaturated possesses a high Gibbs free energy; the overall energy of the system would be reduced by segregating solute from the solution. This reduction of Gibbs free energy is the driving force for both nucleation and growth. The change of Gibbs free energy is dependent on the concentration of the solute [5].

Without supersaturation there would not be a change in Gibbs free energy and no nucleation would occur. When the concentration is greater than the solubility, nucleation occurs spontaneously [2].

However, this energy reduction is counter balanced by the introduction of surface energy, which is accompanied with the formation of a new phase, i.e. forming a nucleus.

The newly formed nucleus is stable only when its radius exceeds a critical size. A nucleus smaller than this critical size will dissolve into the solution to reduce the overall free energy, whereas a nucleus larger than this critical size is stable and continues to grow bigger.

There is also an energy barrier that a nucleation process must overcome as well as the critical radius which represents the minimum size of a stable spherical nucleus.

In the synthesis and preparation of nanoparticles by nucleation from a supersaturated solution, this critical size represents the limit of how small nanoparticles can be synthesized. Optimum conditions require the reduction of: the critical size, the critical energy and the surface energy of the new phase. Temperature can also influence surface energy. Other affecting possibilities include use of different solvents and additives in solution.

Another affecting factor includes the number of growth species per unit volume, which can be used as nucleation centres (in homogeneous nucleation, it equals to the initial concentration). This indicates that a high initial concentration or supersaturation (so a large number of nucleation sites), low viscosity, and a low critical energy barrier are favouring the formation of a large number of nuclei.

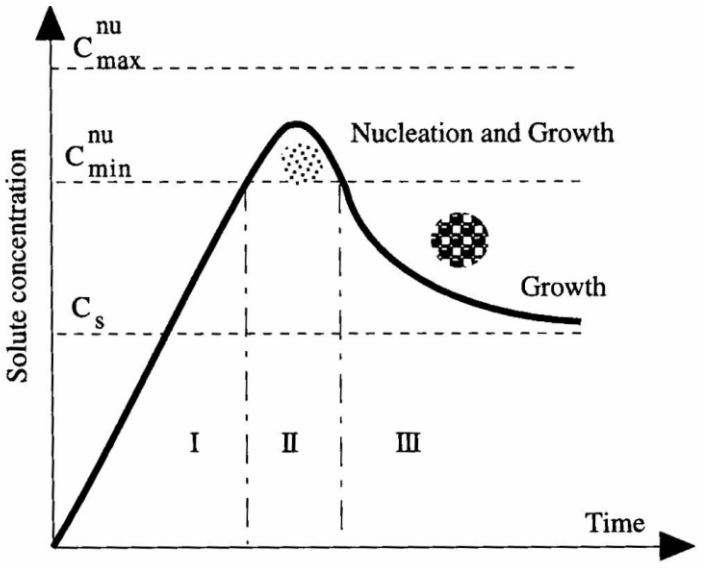

Figure 1.1: Process of nucleation and subsequent growth taken from reference [2]

Figure 1.1 schematically illustrates the process of nucleation and subsequent growth. When the concentration of solute increases as a function of time, no nucleation would occur even above the equilibrium solubility. The nucleation occurs only when the supersaturation reaches a certain value above the solubility.

After the initial nucleation, the concentration (or supersaturation) of the growth species decreases and the change of volume of Gibbs free energy reduces. When the concentration (which corresponds to the critical energy) decreases, no more new nuclei can be formed. Growth of the formed nuclei will proceed until the concentration of growth species reaches the equilibrium concentration or solubility. When the concentration of the growth species increases above the equilibrium concentration, initially there will be no nucleation. However, nucleation occurs when the concentration reaches the minimum saturation required to generate the critical free energy, and the nucleation rate increases very rapidly as the concentration increases further. Although growth process cannot proceed when there is no nucleus, growth rate is above zero for a concentration above its equilibrium solubility. Once

nuclei are formed, growth occurs simultaneously. Above the minimum concentration, nucleation and growth are inseparable processes which occur at different speeds.

1.2.1 Size Distribution

The size distribution of nanoparticles is very important as the optimum conditions for use of nanoparticles is based on their small size and colloidal spacing. The size distribution of nanoparticles can be further altered in the subsequent growth process. The size distribution of initial nuclei may increase or decrease depending on the kinetics of the subsequent growth process. Uniformed sized nanoparticles are achievable by control of the process of growth. There is a direct correlation between size distribution and the growth stages of the nucleus. The growth process of the nuclei is based upon formation of the growth species and diffusion of the growth species from bulk to the growth surface. Another factor which affects the growth process is the adsorption of the growth species onto the growth surface.

If the number of growth species reaches below the minimum concentration required for the process of nucleation, it will stop. However, growth will continue. Diffusion based growth rate for growth species from the bulk solution to the particle surface will either increase or decrease as time elapses due to lack of product for adsorption. The other option is that particles grow bigger as diffusion continues. The diffusion controlled growth is ultimately the ideal form of synthesis as it generates monosized NPs based on the nature of diffusion trying to ensure equilibrium within the system.

When the diffusion of growth species from the bulk to the growth surface is sufficiently rapid, (i.e. the concentration on the surface is the same as that in the bulk), the growth rate is

controlled by the surface process. There are two mechanisms for the surface processes: mononuclear growth and poly-nuclear growth. For the mononuclear growth, the growth proceeds layer by layer; the growth species are incorporated into one layer and proceeds to another layer only after the growth of the previous layer is complete. There is sufficient time for the growth species to diffuse on the surface. During poly-nuclear growth, which occurs when the surface concentration is very high, surface process is so fast that second layer growth proceeds before the first layer growth is complete. The growth rate of particles is independent of particle size or time.

It is obvious that a diffusion controlled growth mechanism is required for the synthesis of monosized particles by homogeneous nucleation. When the nuclei are small, monolayer growth mechanism may dominate, whereas poly-nuclear growth may become predominant as the nuclei become bigger. Diffusion is predominant for the growth of relatively large particles. Of course, this would only be the case when no other procedures or measures were applied to prevent certain growth mechanisms. Different growth mechanisms can become predominant when favourable growth conditions are established.

For the formation of monosized nanoparticles, diffusion-limited growth is desired. There are several ways to achieve diffusion-limited growth. For example, when the concentration of growth species is kept extremely low, diffusion distance would be very large and consequently diffusion could become the limiting step. Increasing the viscosity of solution is another possibility. Introduction of a diffusion barrier such as a monolayer on the surface of a growing particle is yet another approach. Controlled supply of growth species offers another method to manipulate the growth process.

This highlights the importance of the nucleation phase and the stabilisation of the growth of the nanoparticles. One phenomenon that could potentially upset the control over the size of the nanoparticles is the Ostwald ripening theory [6]. Any first-order phase transformation process results in a two phase mixture composed of a dispersed second phase in a matrix. However, as a result of the large surface area present, the mixture is not initially in thermodynamic equilibrium. The total energy of the two-phase system can be decreased via an increase in the size scale of the second phase and thus a decrease in total interfacial area [2]. The unstable surface molecules often go into solution, shrinking the particle over time and increasing the number of free molecules in solution. When the solution is supersaturated with the molecules of the shrinking particles, those free molecules will redeposit on the larger particles. Thus small particles decrease in size until they disappear and large particles increase in size. This shrinking and growing of particles will result in a larger mean diameter for particle size distribution (PSD) [7].

When nanoparticles are around certain chemical agents such as surfactants, the surface and/or surface attributes can be altered. These are usually used to protect the said substances from aggregating or coagulating by conserving particle charge and by modifying the outmost layer of the particle. Depending on the growth history and the lifespan of a nanoparticle, complex compositions can be produced. Possibilities of complex mixtures with adsorbates have to be expected. Aside from adsorbates, these aggregates are usually formed by perikinetic aggregation (the formation of random clusters due to Brownian motion of colloidal particles) or orthokinetic aggregation (this type of aggregation refers to contact or collisions of colloidal particles resulting from bulk fluid motion, such as stirring) [8].

1.3 Semi-Conductors

All solids can be classified as insulators, semiconductors or conductors according to conduction of electrons. An explanation coined for these differences is known as band theory. This is in regards to electrical properties and it accounts for the availability, or non-availability of these conductive electrons. There are large amount of electrons in a solid mass and although the bands actually consist of very large numbers of closely packed discrete energy levels, the bands become essentially continuous. Only the two uppermost bands are considered. These are known as the valence band and the conduction band. The electrons with lower energy levels are described as occupying the valence band. The innermost electrons in an atom are much less influenced by neighbouring atoms, and occupy discrete energy levels. They are sometimes considered to be bound [9]. At higher levels in the valence band electrons can, in fact, move from atom to atom, but only up to the top of the valence band. Since they are permitted only to swap places with other valence electrons in neighbouring atoms, they are effectively unavailable for conduction [9].

Electrons fill the valence band from the lowest level to the highest. The only way that an electron can move from one atom to another in an insulator or semiconductor would be to occupy a slightly different energy level in a neighbouring atom. However, all those energy levels are already full. As discussed above, the electrons may effectively swap places, but in order to facilitate conduction, they must leap up to the conduction band. An energy level band must have some space within it in order for there to be any net movement of electrons within the material. For a material to be able to conduct electricity it must have electrons in its conduction band or spaces in its valence band [9]. There is a zone of forbidden energy levels in insulators and it divides the valence band and the conduction band. The forbidden zone, of the order of 2 electron volts or even less is so large that it is not normally practicable

for there to be sufficient energy to move electrons across it from the valence band to the conduction band. Contrastingly, conductors only have one band, and the top of this band is only partially filled, permitting electrical conduction. This means that there are plenty of nearby energy levels available for electrons to move into. They can flow easily from one atom to another when a potential difference is applied across the conducting material.

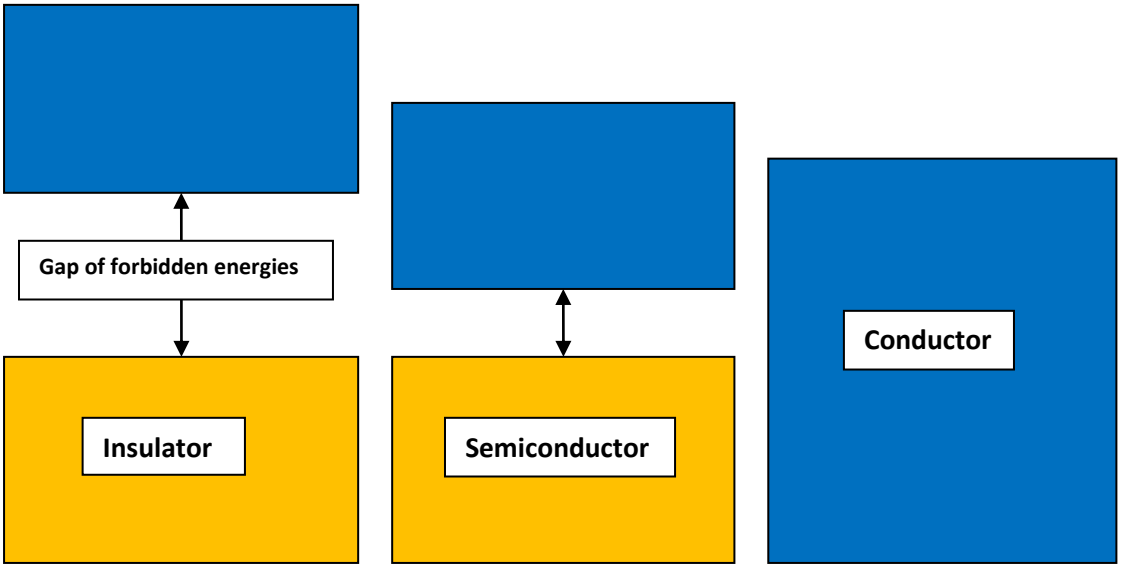

Figure 1.2: A schematic representation of the band gap theory. Reproduced from reference [9]

Like insulators, semiconductors have a completely full valence band and so electrons are not able to facilitate conduction at low temperatures. However, for semiconductors as seen in Figure 1.2, the forbidden energy level zone between the two bands is sufficiently small to make it much easier for significant numbers of electrons to move across this gap and go from the valence band to the conduction band [9].

Classification of semiconductor materials is divided based on the periodic table group which their constituent elements belong to. The group XII-XVI semiconductors are materials whose cations are from the group XII and anions are from group XVI in the periodic table as seen in Figure 1.3. Some examples of group XII- XVI semiconductor materials are cadmium sulfide

(CdS), zinc sulfide (ZnS), cadmium telluride (CdTe), zinc oxide (ZnO), and mercury sulfide (HgS) among others [9].

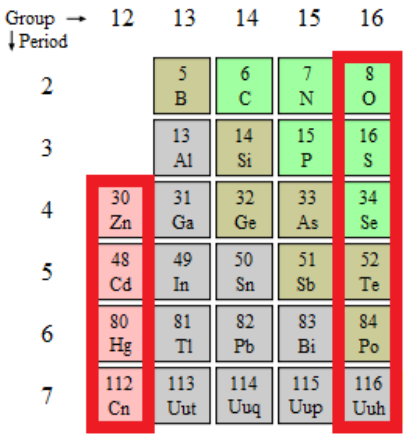

Figure 1.3: The red boxes indicate group 12 and group 16 periodic table elements. Figure reproduced from reference [9]

Semiconductor nanoparticles have many potential applications in the area of demonstration devices, such as light-emitting diodes [2] [10], photocatalysts [11], and electrochemical cells [12]. The transition between semiconductor technologies to nanoscale devices has anticipated improved properties and resolution, e.g. fluorescence labelling, scanning probe microscopy and confocal microscopy. In medicine, greater understanding of the origin of diseases on the nanometre scale is being derived, and drug delivery through functionalised nanostructures may result in improved pharmacokinetic and targeting properties [1].

As mentioned earlier, nanoscale materials often show behaviour which is intermediate between that of a bulk solid and that of an individual molecule or atom. An inorganic nanoparticle is said to contain a few atoms or molecules. This will cause it to act differently to a single atom, despite it being smaller in comparison to a macroscopic solid, hence will show different properties. If the chemical reactivity of a bulk solid was to be compared to that of a nanoparticle, the nanoparticle would have a higher reactivity due to a significant fraction of the total number of atoms being on the surface of the particle [13]. Properties such as

boiling point, melting point, optical properties, chemical stability, electronic properties, etc. are all different in a nanoparticle as compared to its bulk counterpart. In the case of group XII- XVI semiconductors, this reduction in size from bulk to the nanoscale results in many size dependent properties such as varying band gap energy, optical and electronic properties.

1.4 Mercury Sulfide Nanoparticles

Mercury sulfide exists in two crystalline forms, α-HgS which is known as red cinnabar and β-HgS which is known as black metacinnabar. Mercury chalcogenides have been reported to be promising materials as catalysts, ultrasonic transducers, infrared detectors [10] and use in electrochemical cells [10].

The earliest known synthesis of HgS is from the residents of East India (since the seventh century B.C) who used mercury and its sulfide as medicine. The black powder obtained at the end of forty eight hours of milling is found to be finer than 10 nm. The synthesis of the red sulfide of mercury required additional steps of heating and subsequent milling [14].

Mercury is a global contaminant of concern due to its transformation by microorganisms to form methylmercury, a toxic species that accumulates in biological tissues. The production of the neurotoxin methylmercury in the environment is partly controlled by the bioavailability of inorganic mercury Hg (II) to anaerobic bacteria that methylate Hg (II). In sediment pore water, Hg (II) associates with sulfides and natural organic matter to form chemical species that include organic-coated mercury sulfide nanoparticles [15]. Details are needed on mercury sulfide nanoparticles to understand how they are being formed naturally. Despite this interest, there have only been a small number of publications due to the toxicity problem of mercurides [15].

Nevertheless, conventional methods for the preparation of mercury chalcogenides include solid state reactions of metal cations with hydrogen chalcogenides as well as sonochemical methods. Sonochemical methods have been researched and are the effect of sonic waves and wave properties on chemical systems [16]. Advantages of this method include a rapid reaction rate, controllable reaction conditions and the ability to form nanoparticles with uniform shapes, narrow size distributions and high purity [16]. Nanoparticles are popular alternatives to organic dyes as fluorescent labels for biological imaging and sensing due to their small size, tuneable emission, and photostability.

Over the last few years, new methods have been developed in preparing HgS, having nanoscale dimensions with the goals of searching for milder preparation conditions and avoiding the use of toxic reagents or complicated organometallic precursors. The previous methods usually required high temperatures (around 800 K) and/or involved the use of toxic and highly sensitive precursors. Solution based synthesis is more promising in terms of cost and potential for high volumes for production rather than solid state reactions and gas phase chemical processes.

Mahapatra *et al* synthesised HgS in 1 hour using ammonia, PVA, mercury chloride ($HgCl_2$) and thiourea as the precursor [17] while Patel *et al* synthesized nanoparticles, average crystalline size of HgS being 15 nm [18].

Wang *et al* reported a methodology in which mercury acetate and sodium selenosulfate reacted in water at 70°C to synthesise mercury sulfide nanoparticles in over 24 hours [19], proving that mercury sulfide nanoparticles can be produced under ambient conditions using a simple precipitation method. Wang *et al* have shown α-HgS nanoparticles with sizes of 10-13 nm while β-HgS are around 11-15 nm. Wang *et al* have further developed this idea and had another method in synthesising HgS nanoparticles involving the use of thiourea which

synthesized nanoparticles in 30 minutes. Again, sonication and bubbling nitrogen gas were needed. The temperature was raised to 70°C and black precipitate was formed.

Mahapatra *et al* have synthesised nanocrystals in around 60 minutes [17]. HgS nanoparticles have electrochemical traits which allow them to be very good semiconductors as Wang *et al* have noted. α-HgS is a wide band gap semiconductor. Above 344^{o}C temperature, α-HgS exhibits a zinc-blend modification while β-HgS is a narrow band gap semi-metal. As mentioned earlier, a wider band gap usually refers to less efficient conducting properties for the medium. These materials have immense potential applications in light-emitting diodes, optical detectors, solar cells and other photoelectric devices. The fundamental application problem of these semiconducting NPs is connected with the insufficient stability of their dispersions and generation of large aggregates when dry, that leads to loss of their special nanoscale properties.

It is known that sonication helps to decrease the particle size and make the product more stable, compared to the conventional method [16]. The application of ultrasonics to nanomaterials has positive effects. The most obvious being the dispersion of materials in liquids in order to break particle agglomerates formed via orthokinetic or perikinetic aggregation. Another process is the application of ultrasound during particle synthesis or precipitation. Generally, this leads to smaller particles and increased size uniformity [16].

In aqueous media, the nanosized particles are mainly dispersed by the ionic repulsion forces generated due to different adsorbed species on their surface. In this context, surfactant-supported stabilisation of the nanoparticles in aqueous solution has proven to be one of the most effective methods. In contrast to their bare counterparts, these nanoparticles remain well

dispersed in solution for a long time. Various surfactants can tune nanoparticles shape, size and other surface properties.

There now seems to be a growing concern for mercury sulfide nanoparticles to be monodispersed, produced on a large scale, and remain cost efficient within the correct size range. For this reason, the aim to synthesise HgS nanoparticles in a more effective manner than those mentioned before is needed. The problem of precipitation is to be addressed and colloidal particles are to be produced within the specified size range and in short time.

1.5 Introduction to Cadmium and Bismuth

Cadmium sulfide (CdS) is an important group II–VI semiconductor with many excellent physical and chemical properties, which has promising applications in multiple technical fields including photochemical catalysis, gas sensor [19] detectors for laser and infrared [20], solar cells [21], nonlinear optical materials [22], various luminescence devices [23] and so on. In the last few decades, efforts have been devoted to the preparation of high quality CdS nanoparticles and the investigation of optical properties. The possibility of tuning the properties of particles by controlling their sizes and shapes implies search of new experimental methodologies that yield very low size and shape-dispersion nanoparticles [24].
One of the factors which make cadmium so promising is its photocatalytic nature. This exploits the semiconductor as a photocatalyst, using this as a promising method for the treatment of contaminated ground, surface, and waste waters containing various organic pollutants [25]. This method is clean, requires low temperature and is a non-energy intensive approach for treatment of pollutants. Among semiconductors, TiO_2 and ZnO are considered to be the most suitable for photocatalytic degradation of pollutants due to their chemical inertness [37] and greater resistance to photo-corrosion [26]. However, they have several

limitations. Ultraviolet light is required for their photocatalytic activities. Only about 3% of the solar spectrum consists of UV light and employing TiO_2 and ZnO for such purposes means inefficient utilisation of solar energy. Instead, utilisation of sunlight for such purposes would be cost effective. Therefore, there is a need to look for other nanomaterials which possess good photocatalytic properties in the visible range [27].

Previous literature about the preparation of CdS nanoparticles took around 2 hours to form particles around 10 nm in diameter [28].

While uses of cadmium seem to focus upon its optical properties, new uses for bismuth sulfide nanoparticles have been found. Bismuth sulfide nanoparticles are being used to target blood clots by targeting fibrin in the blood stream [29]. Previous literature about the formation of bismuth sulfide nanoparticles showed an average diameter of around 40-50 nm. The method involved 0.5 grams of bismuth granules being added to 30 mL of paraffin oil in a flask and heated at 280°C for 10 hours and stirred. The supernatant was then transferred to another flask and cooled down to room temperature [30]. It was then centrifuged and washed with chloroform to get black-brown powder.

Images showed wide ranging nanoparticle sizes, the average size being 50 nm. The particles were spherical in shape as seen in figure 1.4. This is a very long and tedious method.

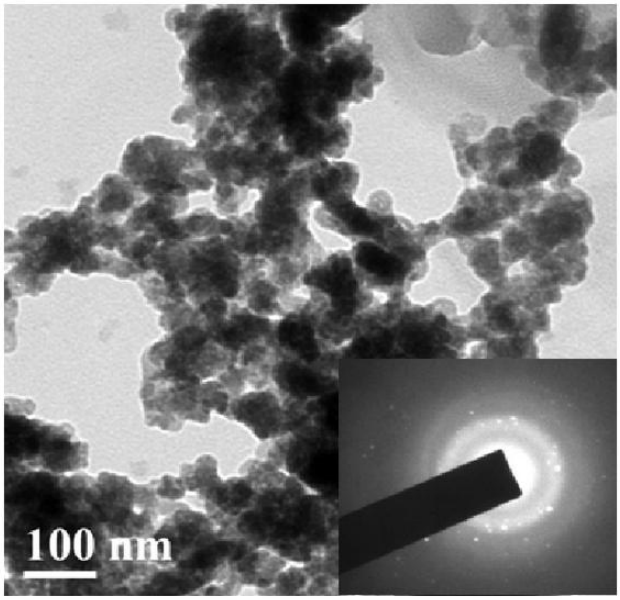

Figure 1.4: TEM image of bismuth sulfide nanoparticles which shows the size and morphology. Taken from reference [30]

In this thesis, a novel methodology to produce mercury chalcogenides is presented which is then shown to be extendable to other metal chalcogenides. This method is quicker than previous literature and produces nanoparticles which fit the criteria for being perfectly synthesised. These include monodispersion, quick synthesis and stability. This method is novel as it differs greatly from the contemporary methods of synthesis. There are no previous reports of a direct injection of a precursor into a metal solution under ambient conditions. This solution based method reduces the direct contact with harmful chemicals described in previous research [14] [15]. The milling method poses a risk of inhalation [14]. Solution based synthesis also eliminates the need of constant heating as described by previous research [17] [32]. The overall toxicity of the solution based method is reduced because HgS is more stable in acidic conditions due to its unique solubility constant (Ksp). Mercury hydroxide, which is the main product in the experiment remains as an insoluble precipitate in acidic conditions. It has a value of $3.6 \times 10^{-26} mol^3/L^3$ [19]. Previous literature tends to synthesise the NPs in alkali conditions [17]. What makes this experiment so unique is the use of Nafion to

stabilise the particles and to prevent coagulation for over 1 week, which is great when compared to contemporary research.

2. Experimental Details

All chemicals were obtained from Sigma Aldrich at the highest purity available. Specifically, these were: mercury (II) nitrate (99.9%), nitric acid (70%, purified by redistillation, ≥99.999% trace metals basis), perfluorinated Nafion®resin exchange, sodium cholate (97.9%), 1- butanol (ACS reagent 99.4%), sodium citrate dihydrate (>98%) and thioacetamide (99.9%ACP).

HgS nanoparticles were prepared from 0.5 M aqueous $Hg(NO_3)_2$ being added into distilled water, acidifed with $HNO_3$to pH=2. Next 0.5 M aqueous thioacetamide was spiked into the buffer causing the solution to instantly turn black. The black colour indicates that the HgS nanoparticles were produced. This process was repeated, however the distilled water containing $Hg(NO_3)_2$ was adjusted to pH=4.

Individual 10 mL vials of synthesised HgS were prepared using the above method and a range of surfactants were added. The surfactants added into each respective vial are as follows: 500 µl of Nafion was added into a 10 mL vial of HgS, 500 µl of butanol was added into a 10 mL vial of HgS, 0.5 M of sodium citrate was added into 10 mL HgS (0.294 mg), 0.5 M ethylenediaminetetraacetic acid (EDTA) in 10 mL of HgS (0.374 mg) and 0.5 M of sodium cholate was added into a 10 mL vial of HgS (0.430 mg).

High purity standards of cadmium and bismuth were purchased from Fisher Scientific, Cd^{2+} 1000 ppm, 2% HNO_3 and Bi^{+2} 1000 ppm, 2% HNO_3 respectively.

During the preliminary tests, a solution containing 1 gram of sodium sulfide and 1 litre of distilled water was prepared. 300 µl of sodium sulfide was added into a 300 µl vial of

bismuth standard at 1000 ppm with 2% HNO_3. 300 µl of thioacetamide solution was spiked into a separate vial containing 300 µl of bismuth standard.

Using a solution containing 1 gram of sodium sulfide and 1 litre of distilled water, 300 µl of sodium sulfide was added into a 300 µl vial of cadmium standard at 1000 ppm with 2% HNO_3. 300 µl of thioacetamide solution was spiked into a separate vial containing 300 µl of cadmium standard.

Next, 181 µl of sodium sulfide solution was spiked into 300 µl of bismuth standard and the colour change and coagulation rates were observed. In a separate vial, 160 µl of sodium sulfide solution was spiked into 300 µl of cadmium standard and the colour change and coagulation rates were again observed.

Finally, the experiments were repeated and 300 µl Nafion was spiked into each vial. All experiments were conducted in a sonication bath.

A Jeol 5600 scanning electron microscope (SEM) was used to image the particles and it was fitted with an energy dispersive x-ray analyser (EDX) to identify elements. The scanning electron microscope (SEM) uses a focused beam of high-energy electrons to generate a variety of signals at the surface of solid specimens. The signals that derive from electron-sample interactions reveal information about the sample including external morphology (texture), chemical composition, and crystalline structure. The SEM is critical in all fields that require characterisation of solid materials. The only known limitations are that the SEM cannot detect very light elements such as H, He or Li. Also, samples must be solid and they must fit into the microscope chamber. The maximum size in horizontal dimensions is usually on the order of 10 cm and samples must be stable in a vacuum.

A Zeiss manu supra 40vp TEM (Transmission electron microscopy) was used to image the particles. TEM is a microscopy technique whereby a beam of electrons is transmitted through an ultra-thin specimen. TEM allows imagery of the inside of the specimen. The main differences between the techniques are that TEM has a much higher resolution than SEM. Also, SEM provides a 3-dimensional image while TEM provides a 2-dimensional image.

EDX is an x-ray technique used to identify the elemental composition of materials. EDX systems are attachments to SEM and TEM instruments where the imaging capability of the microscope identifies the specimen of interest. The data generated by EDX analysis consist of spectra showing peaks corresponding to the elements making up the true composition of the sample being analysed.

3. Results and Discussion

3.1 HgS Synthesis at pH=2

HgS nanoparticles synthesised by spiking thioacetamide into the acidified water caused the solution to instantly turn black. This is an indication of their formation confirmed by previous literature [10].

Mercury (II) hydroxide can only exist as an insoluble precipitate suspended in a solution. This is due to high concentration of H^+ and a low concentration of OH^-. This causes the reaction to move to the right so mercury ions (Hg^{2+}) remain soluble. The solubility constant (*Ksp*) of mercury hydroxide is 3.6 x$10^{-26}$$mol^3/L^3$. *Ksp* being expressed as:

$Ksp = [Hg^{2+}] [OH^-]^2$.

$$Hg^{2+} + 2H_2O \rightleftharpoons Hg(OH)_2(s) + 2H^+$$

$$Hg(OH)_2\,(s) \rightleftharpoons Hg^{2+}(aq) + 2OH^-\,(aq)$$

Scheme 1: Reaction mechanism of Hg^{2+} in water

At pH=7 the concentration of hydroxide ions is same as proton ions *i.e.* 10^{-7} M. For precipitation to occur there needs to be a value of 3.6 x10^{-12} mol^3/L^3. This fulfils the criteria required and begins precipitation as shown in Scheme 1.

Scheme 2: Reaction mechanism of thioacetamide in water

Scheme 2 illustrates how thioacetamide is hydrolysed and one of the by-products is hydrogen sulfide. This reacts in solution to form hydrogen sulfide ions. These ions are further hydrolysed, producing sulfide ions.

Scheme 3: Reaction mechanism of hydrogen sulfide in water

The more acidic the pH, the slower sulfide ions are formed as shown in scheme 3. This is due to large amounts of H^+ present from the high acidity of the solution; therefore, there is a high concentration of H_2S due to the equilibrium:

But this is prevented due to protons.

Sulphur ions are produced, contributing to the formation of mercury sulfide.

Mercury sulfide was fabricated as described in the experimental chapter and was imaged via SEM. Figure 3.1 shows the different peaks present which confirm the purity of the synthesised nanoparticles. Figures 3.2a, 3.2b and 3.2c show SEM images of the synthesised particles which appear to have coalesced. The images depict HgS nanoparticles synthesised at pH=2 and are at varying magnifications.

It is difficult to see individual particles in Figures 3.2a and 3.2b. Closer inspection of Figure 3.2c reveals the formation of nanoparticles which are very difficult to see individually. The reason behind this could be that the concentration of nanoparticles is far too high. The next idea was to change the concentration of the mercury by diluting the samples prior to SEM examination. This is evident in Figure 3.2d. Copper has peaked on the EDX. The reason for this is, when the sample was being analysed to confirm that HgS was synthesised, the copper substrate used for the nanoparticles is likely to have been detected.

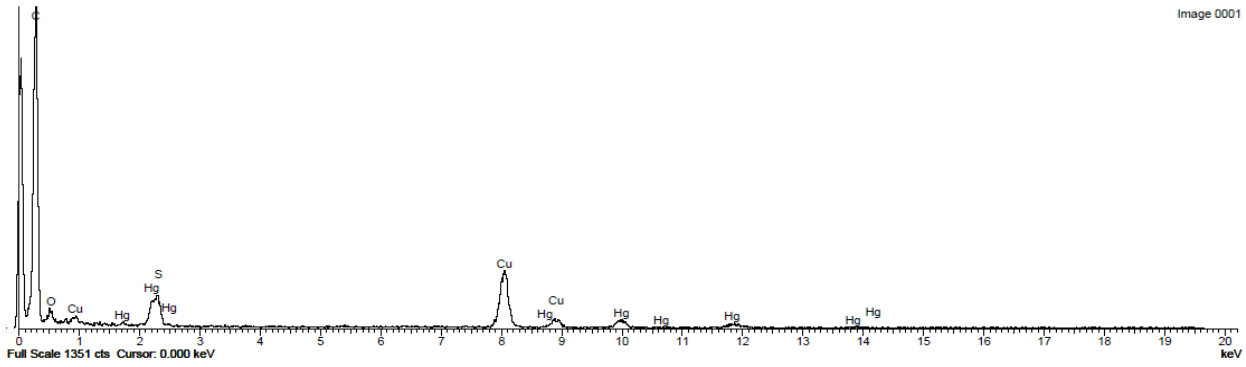

Figure 3.1: EDX of HgS synthesised at pH=2

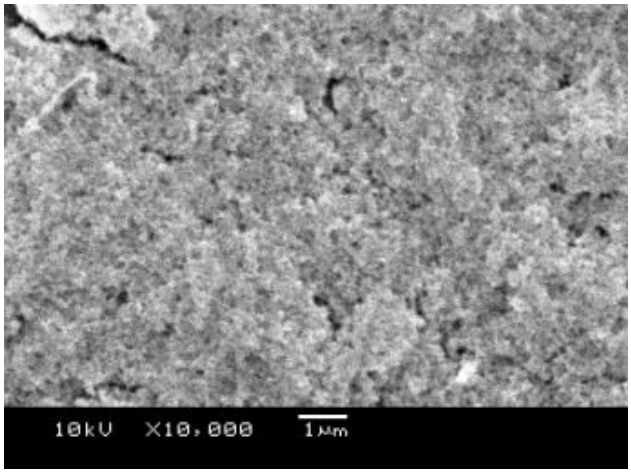

Figure 3.2a: SEM image of the synthesised HgS pH=2 nanoparticles

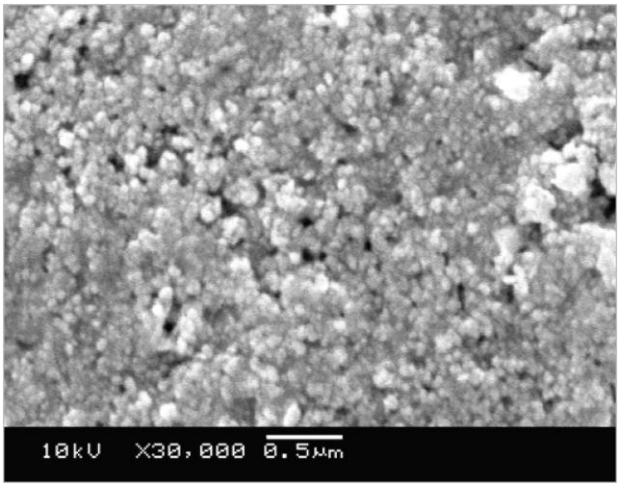

Figure 3.2b: SEM image of the HgS nanoparticles synthesised but have coalesced

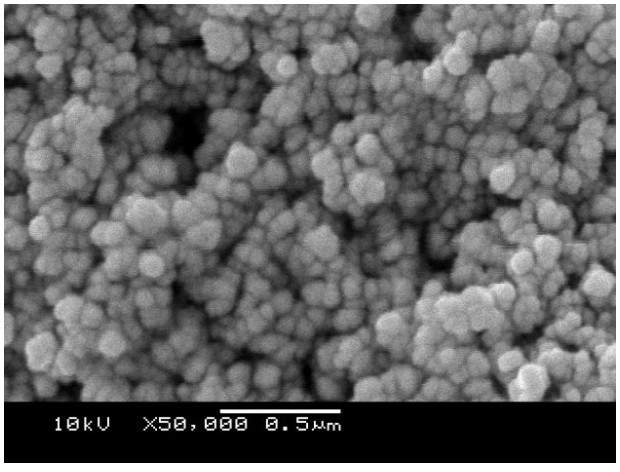

Figure 3.2c: SEM image of the synthesised HgS nanoparticles but have coalesced

TEM images of the synthesised particles were also obtained, which are shown in Figures 3.3a, 3.3b and 3.3c. It is evident that the particles are in the range of 8-12 nm in diameter. The sample was diluted to 1/5th of its original concentration, using ethanol before imaging. The NPs were synthesised within a few minutes and appear very monodispersed in the image. The majority of the particles were the same size. However, it is apparent that a few were greater than the average size and the reason behind this could be based on the adsorbance of free ions or aggregation. It is more likely that the particles have slightly aggregated and TEM imagery confirmed this suspicion. The particles had coagulated slightly at the time of the image.

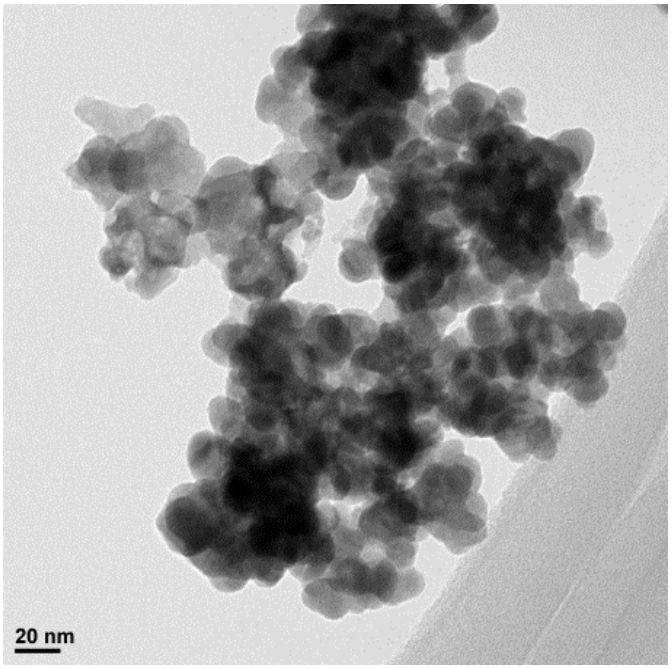

Figure 3.3a: TEM image of HgS nanoparticles showing the size range to be between 8-12 nm

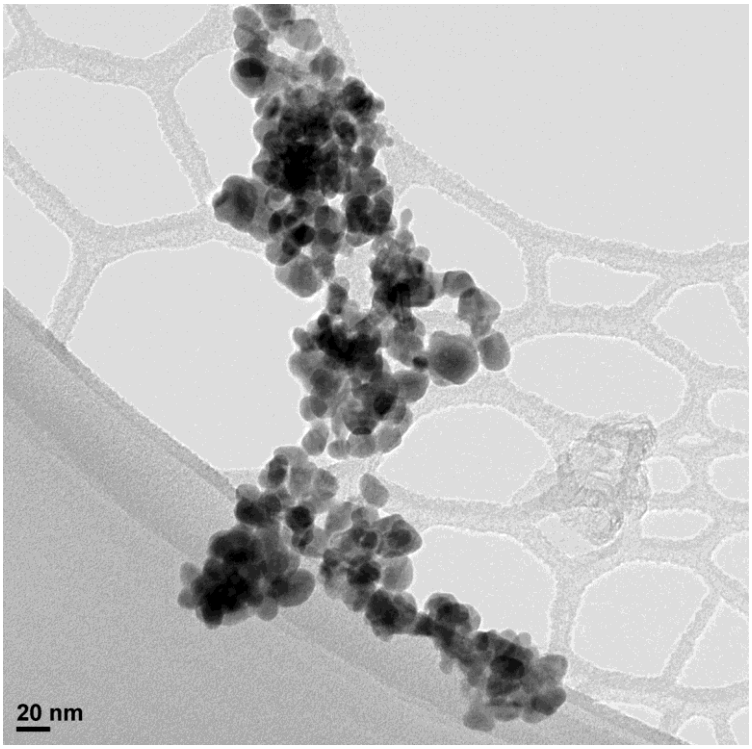

Figure 3.3b: TEM image of HgS nanoparticles

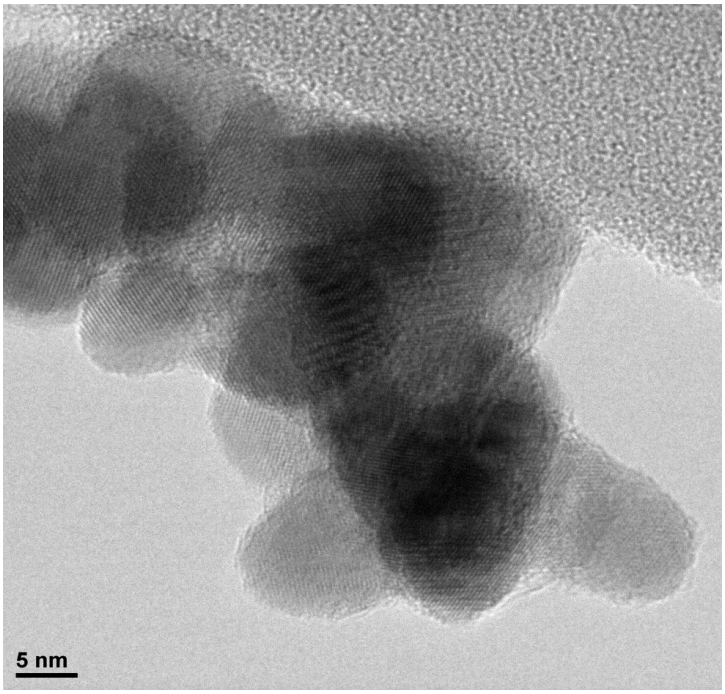

Figure 3.3c: TEM image once coagulation had occurred

Figures 3.3a and 3.3b depict the HgS nanoparticles synthesised in less than 2 minutes. When compared to previous literature there is evidence to suggest that the particle size is within the expected range [17]. It is also difficult to differentiate between individual particles. Figure 3.3c shows that despite particle synthesis within a quick time, aggregation is eventually inevitable.

The next task was to avoid precipitation and aggregation. There are many methods in which this can theoretically be achieved. During experimentation coagulation was a regular occurrence within 10 minutes of synthesis.

3.2 Prevention of Coalescing

3.2.1 EDTA

The following synthesis was performed in order to prevent coalescing. It was likely that an additive would be needed in order to bind the particles in a uniform shape, while maintaining their monodispersivity and without affecting reaction time.

Ethylenediaminetetraacetic acid, widely abbreviated as EDTA is a polyamino carboxylic acid and is colourless.

In an experiment *Han et al* [31] revealed EDTA effectively extracted mercury from cinnabar-contaminated Oak Ridge soils. Hence, it can be inferred that this successful interaction with mercury combined with the structural advantages of EDTA was the reason for its selection in possibly preventing coagulation.

In theory, EDTA should affect the overall reaction between the mercury nitrate and the thioacetamide since the mercury will be complexed with the EDTA. This occurs because EDTA is a complexing agent for metals. Its usefulness arises because of its role as a hexadentate ("six-toothed") ligand and chelating agent. After being bound by EDTA, metal ions remain in solution but exhibit diminished reactivity. EDTA removes toxic metals from the blood. Studies have shown that as people age they continuously accumulate toxic metals: lead, mercury and aluminium etc, substances capable of forming a complex compound with another material in solution [32]. In theory, EDTA can chelate or complex metal ions in a 1:1 ratio (metal: precursor).

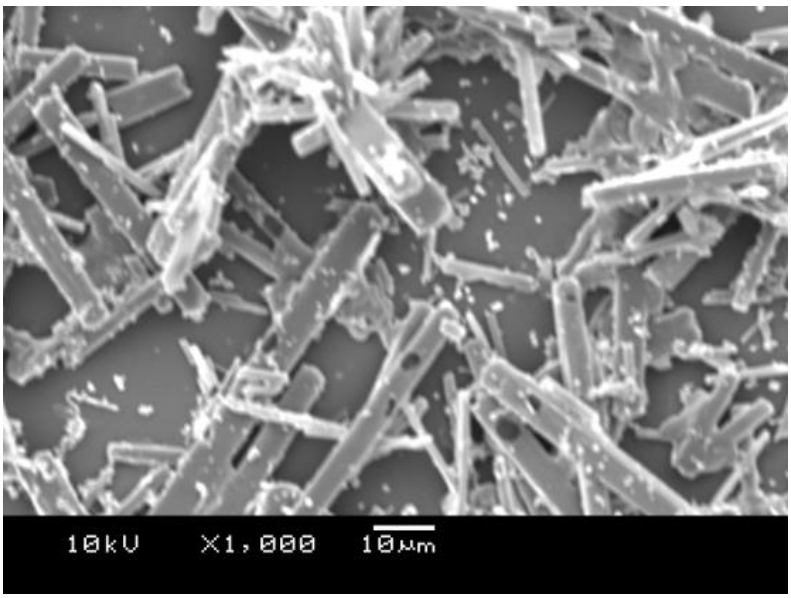

Figure 3.4a: SEM image of EDTA when added to HgS nanoparticles

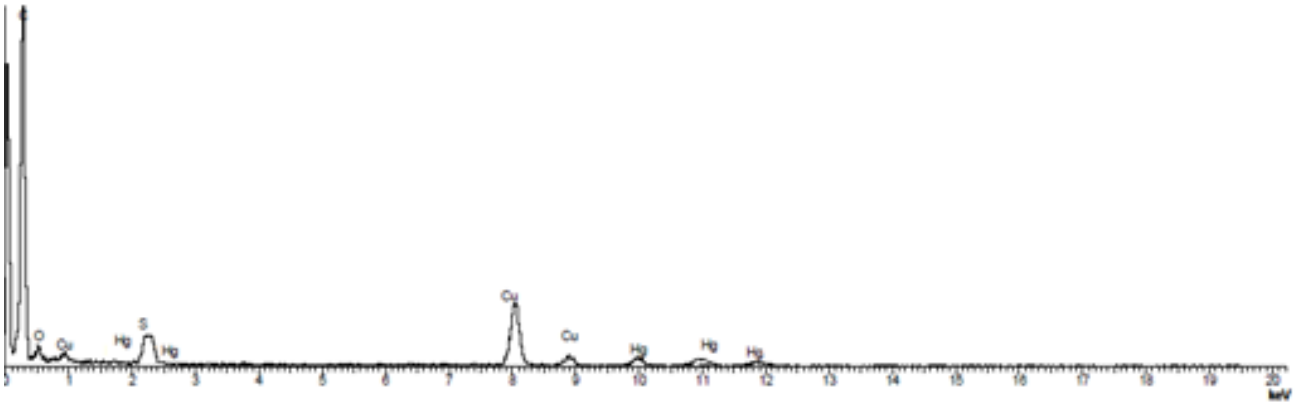

Figure 3.4b: EDX for HgS with the additive EDTA

Figure 3.4a shows the structure of EDTA and how it encapsulated some of the HgS nanoparticles. However, due to the size difference between HgS and the EDTA, a number of the particles were free around the chelating agent and therefore were unaffected. The actual rate of synthesis was not affected with the addition of the EDTA. The only difference was the rate of coagulation. The pH=2 HgS, without the use of additives, fully coagulated within 1 hour of synthesis. With the addition of EDTA, the rate of coagulation was increased by 50%. This may be due to interactions between the HgS and the EDTA or because of larger complexes within the solution adsorbing to increase the size of agglomerates. EDTA research was not required further. Figure 3.4b shows the EDX for HgS with EDTA.

3.2.2 Butanol

The solvent was changed from aqueous to non-aqueous with the addition of butanol. Hydrophobic molecules in water generally tend to aggregate, so minimising their surface contact and associated surface energy with water means hydrophobic molecules cluster together. The theory is, if the nanoparticles are within a hydrophobic medium they will cluster together due to interactions with the water. This will prevent the particles from

precipitating by encapsulating the nanoparticles. In a hydrophobic interaction, it seems as if the hydrophobic molecules are rejecting water. What is actually happening is that water is rejecting the hydrophobic molecules in favour of bonding with itself. Water bonds easily with polar molecules and given that water is characteristically polar, it will have a preference to bond with itself. Figure 3.5a shows the EDX of the HgS with butanol as the surfactant. This confirms the purity of the nanoparticles synthesised. Hg and S are both present.

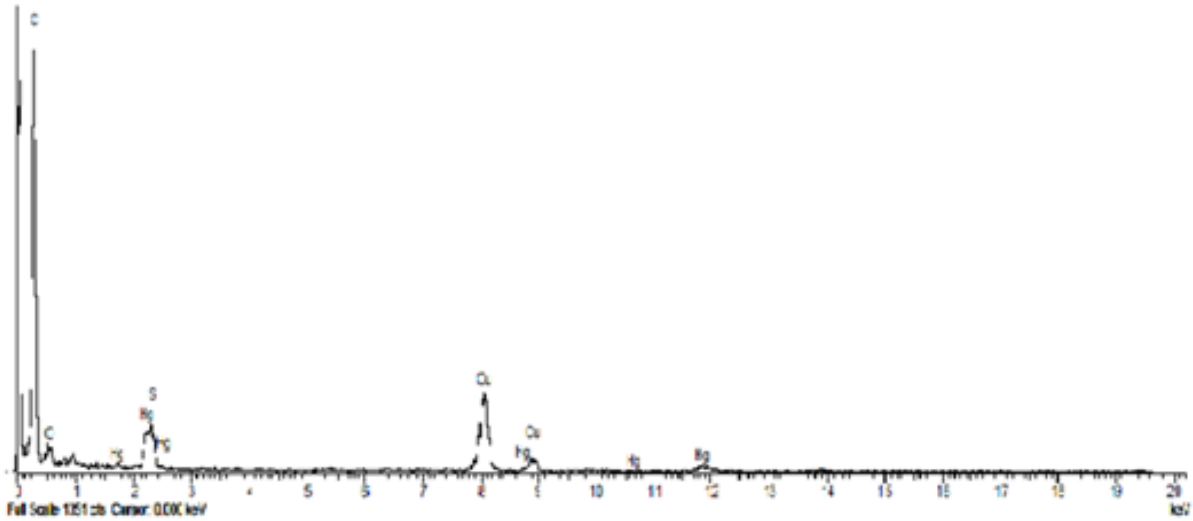

Figure 3.5a: EDX of HgS with the additive butanol

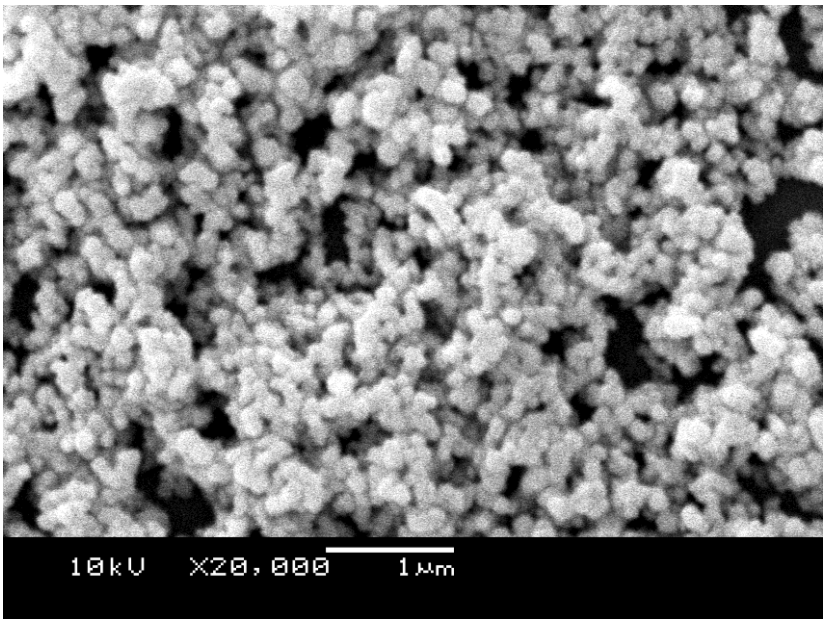

Figure 3.5b: SEM Image of HgS nanoparticles with butanol as an additive

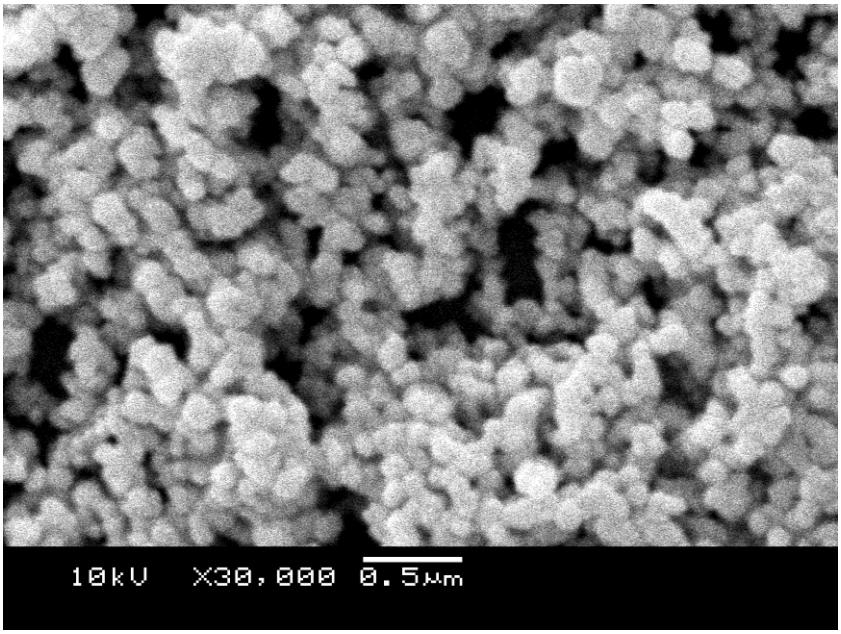

Figure 3.5c SEM image of HgS nanoparticles with the addition of butanol

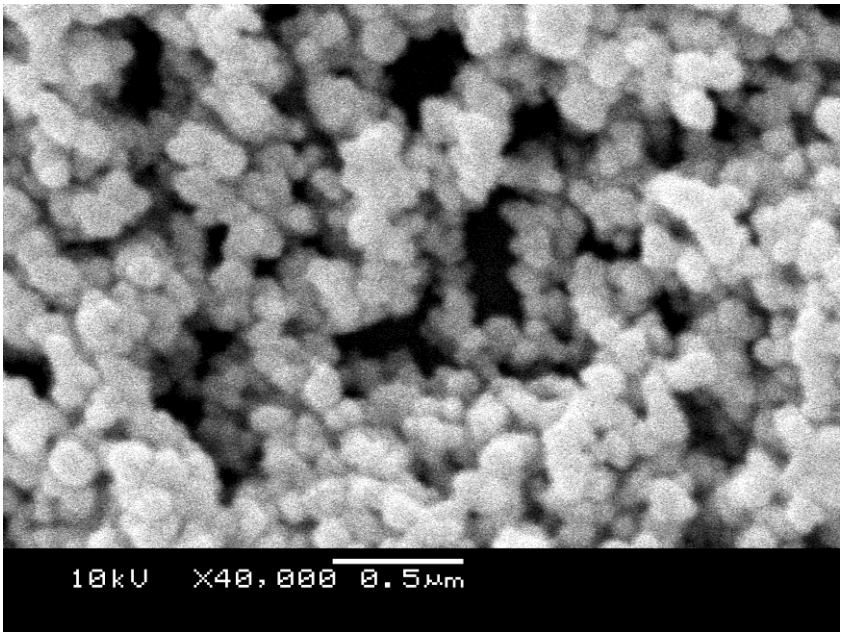

Figure 3.5d: SEM image of HgS nanoparticles with the addition of butanol at x30,000 magnification

Figures 3.5b, 3.5c and 3.5d all show particle size larger than what has been explained in previous literature, with the addition of butanol. However, they were monodispersed and had uniform morphology which accepts the trend set by past research associated to HgS NPs. There were slight signs of coagulation initially and after a short period of time, a layer was formed between the HgS particles and the butanol. There was a divide in the middle of the

beaker which had the precipitated particles on the bottom and butanol on top. It is likely that this was caused by precipitation of the HgS towards the bottom of the vial. As butanol is not soluble in water, clusters are formed towards the top of the vial due to its hydrophilic nature. Figures 3.5b, 3.5c and 3.5d all show a very high saturation of particles.

3.2.3 Sodium Citrate

Sodium citrate was the next option for trying to stabilise the nanoparticles without increasing synthesis time. Trisodium citrate has the chemical formula of $Na_3C_6H_5O_7$. It is sometimes referred to simply as sodium citrate, though sodium citrate can refer to any of the three sodium salts of citric acid. Sodium citrate is used in the stabilisation and the capping of gold nanoparticles in the Turkevich method [33]. Figures 3.6a and 3.6b depict the interactions of the nanoparticles formed with the addition of sodium citrate.

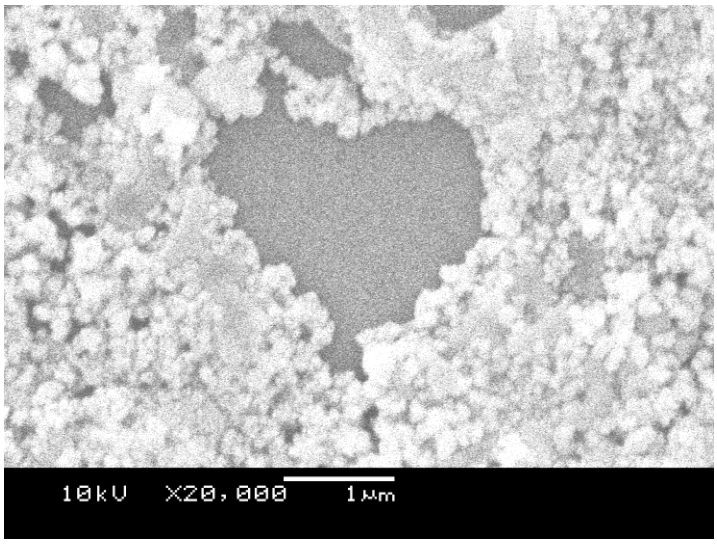

Figure3.6a: SEM image of the HgS nanoparticles with the addition of sodium citrate

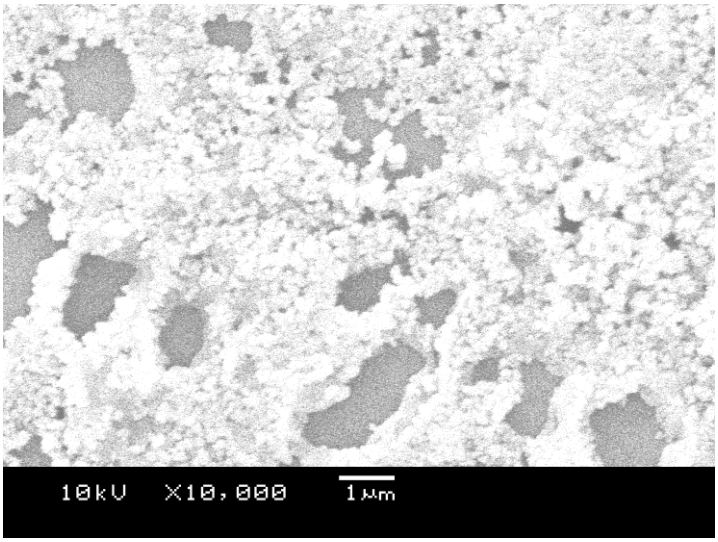

Figure 3.6b: SEM image of the addition of sodium citrate to HgS at x10,000 magnification

Figures 3.6a and 3.6b show the effect of sodium citrate on the formation of HgS nanoparticles. The particles seem to be globular and coagulated. Sodium citrate does not seem to have had any effect on the nature of formation. Also, what is interesting to notice is the EDX (Figure 3.6c) does not seem to show any peaks for sodium. The only justification for that could be that there is an overlap in where the peak should be. Reports suggest that it should peak around 1-1.5 keV [34]. It could be that there was an overlap with the copper coated stubs that the solution was mounted on. This is the most likely explanation as copper has peaked where sodium should have. There is no need to continue to explore the development of sodium citrate.

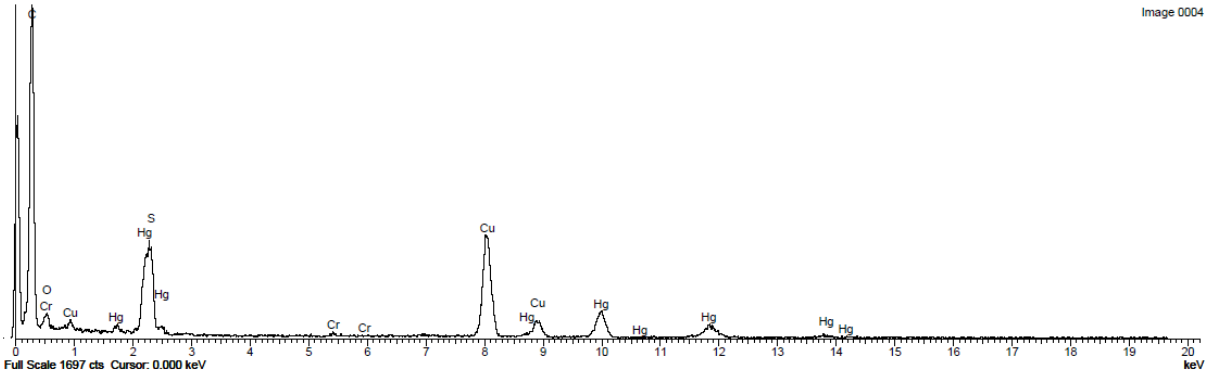

Figure 3.6c: EDX of HgS with the additive sodium citrate

3.2.4 Sodium Cholate

Figure 3.7a: The structure of sodium cholate

Sodium cholate (Figure 3.7a) is a water-soluble, bile-acid commonly used in protein methods such as cell lysis, liposome preparation, isolation of membrane proteins and lipids, preventing nonspecific binding in affinity chromatography and as a cell culture media supplement [25]. It has binding properties and the theory is to see if it can bind nanoparticles and prevent them from coagulating [25].

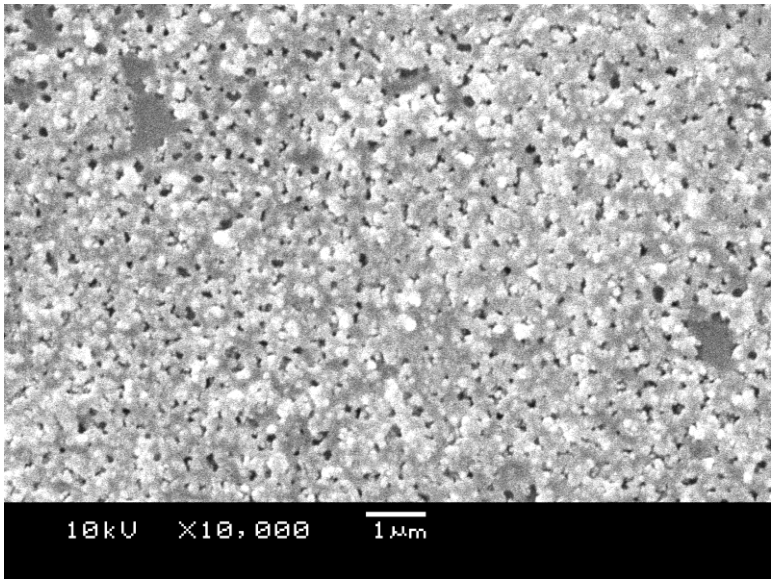

Figure 3.7b: SEM image showing the NPs synthesised and stabalised with sodium cholate

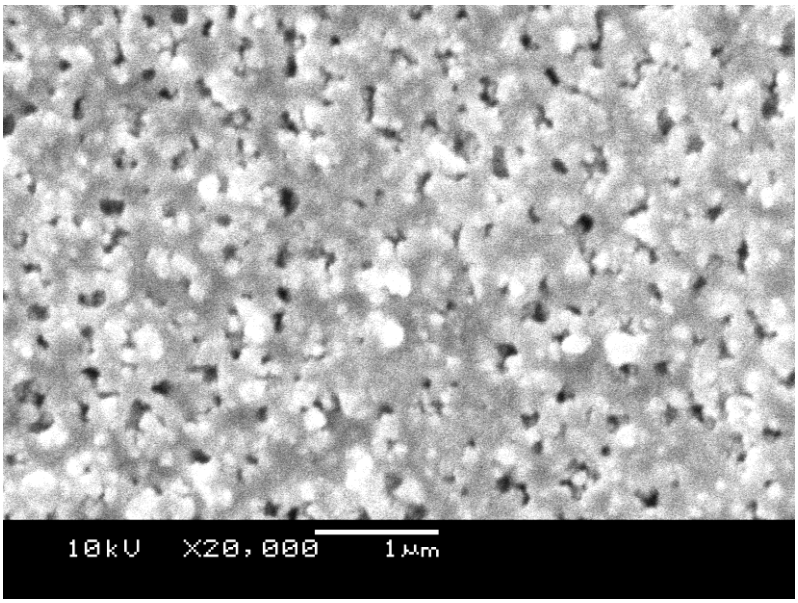

Figure 3.7c: SEM image showing NPs synthesised and stabalised with sodium cholate

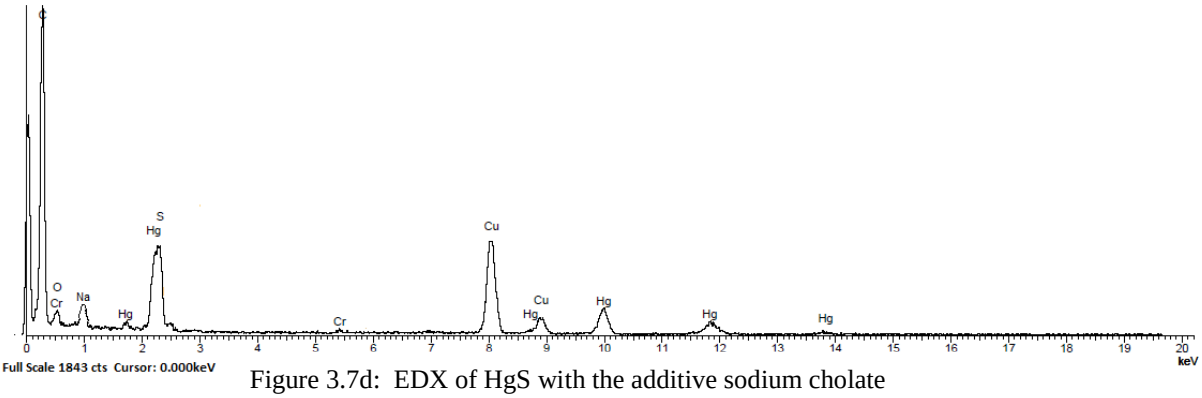

Figure 3.7d: EDX of HgS with the additive sodium cholate

Figures 3.7b and 3.7c show the structure of HgS nanoparticles with an additive of the surfactant sodium cholate. At x10,000 and x20,000 magnification, it is clear that there is a lot of coalescing. It is apparent at x10,000 magnification but is confirmed at x20,000 magnification. The actual particles seem to be the correct size for HgS but the coagulation gives the impression of large particles. Due to coagulation, no further research was required using sodium cholate as an additive. Figure 3.7d shows the EDX of the sample.

3.2.5 Nafion

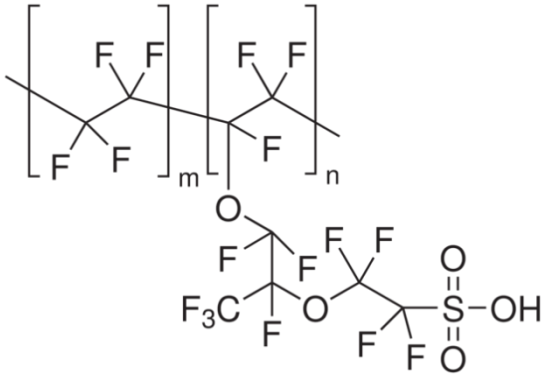

Figure 3.8a: Structure of Nafion

Nafion is a copolymer of tetrafluoroethylene (Teflon®) and perfluoro-3,6-dioxa-4-69er methyl-7some-octene-sulfonic acid as seen in Figure 3.8a. Like Teflon, Nafion is highly

resistant to chemical attack. The premise is that the addition of Nafion will prevent coagulation. The key behind this may lie in the structure of Nafion.

Unlike micro-porous membrane permeation, which transfers water through a relatively slow diffusion process, Nafion removes water by absorption as water-of-hydration.

One of the benefits of using Nafion is that it is not only highly resistant to chemical attack, but also exhibits highly selective absorption and transfer of compounds. The chemical basis of Nafion's superior conductive properties remains a focus of research. Protons on the SO_3H (sulfonic acid) groups "hop" from one acid site to another. Pores allow movement of cations but the membranes do not conduct anions or electrons. Nafion is highly ion conductive. It functions as a cation exchange polymer [26].

The ionomer known as Nafion consists of a perfluororinated backbone and ether side chains terminated with sulfonic groups $–SO_3^-$. Nafion membranes have unique properties with respect to stability, solubility, and ionic conductivity, which make them suitable for a variety of applications [35].

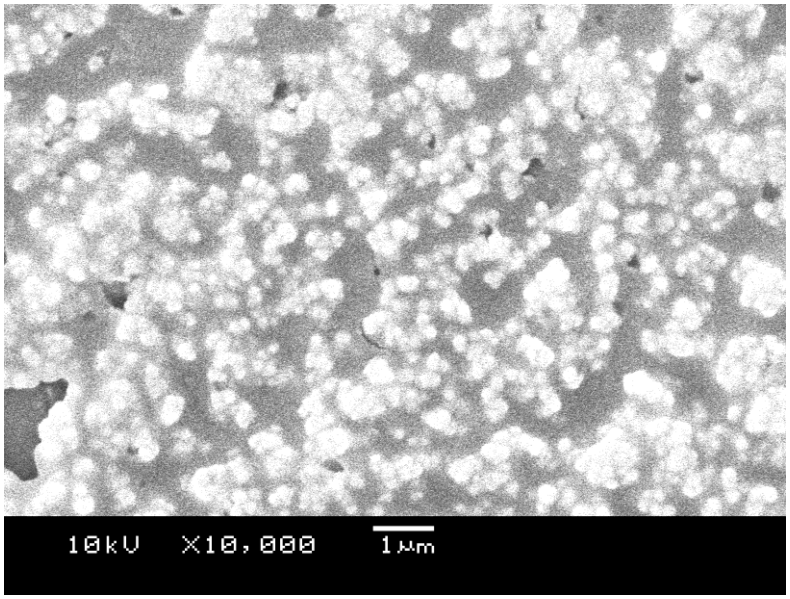

Figure 3.8b: SEM image showing the effect with the addition of Nafion to the HgS

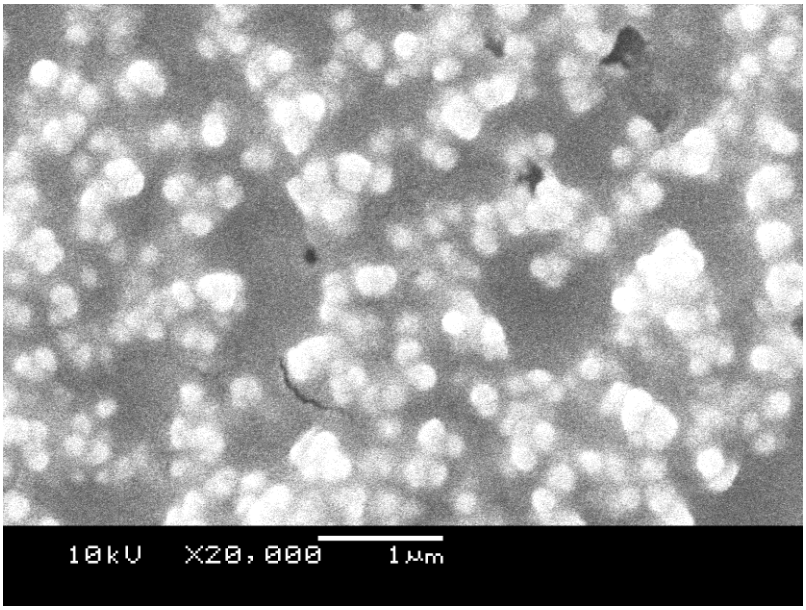

Figure 3.8c: SEM image of HgS nanoparticles with the addition of Nafion to stabilise the particles

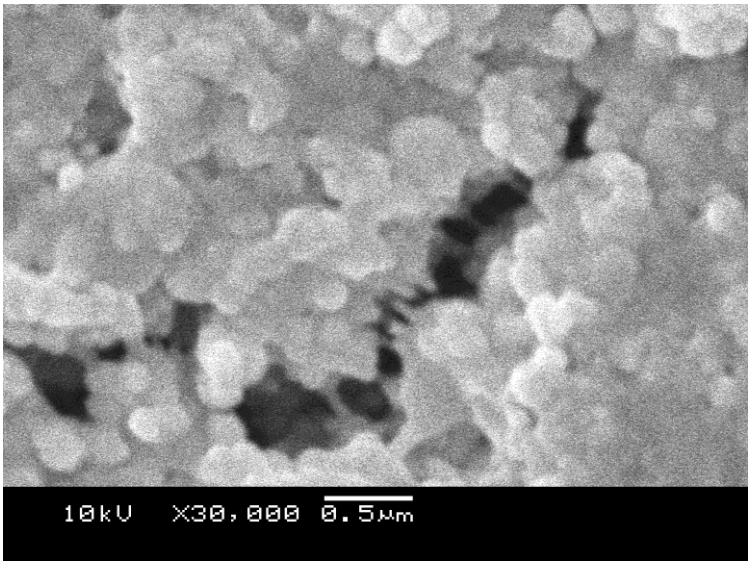

Figure 3.8d: SEM image showing the severity of coalescing for HgS with the addition of Nafion

Figures 3.8b and 3.8c show the structure of HgS nanoparticles with an addition of the surfactant Nafion. Note the fluorescing on the images. This is due to the fluorine within the structure of Nafion. Figure 3.8d was taken 1 week after the initial synthesis when coalescing was apparent. This figure depicts the extent of the coalescing.

It is clear that there is a lot of coalescing. However, despite this, with the addition of Nafion the solution stayed colloidal for over a week. It is clear now that the ionomer Nafion is the best choice for keeping the nanoparticles colloidal.

It was noticed that at pH=2 the particles would stay colloidal for an hour without the use of any surfactant. Once the parameters had changed to pH=4, the particles were colloidal for over a week with only slight signs of precipitation, thus staying in colloid longer than ones reported by M. Elimelech *et al* [7] and other papers. Figure 3.8e shows the EDX of HgS with Nafion. The EDX shows peaks of mercury, sulphur, and small peaks of fluorine.

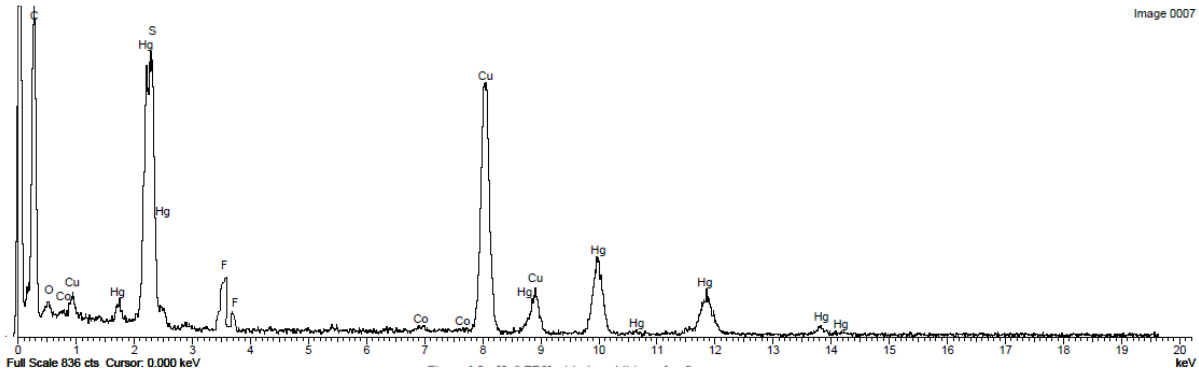

Figure 3.8e: EDX of HgS with the addition on Nafion

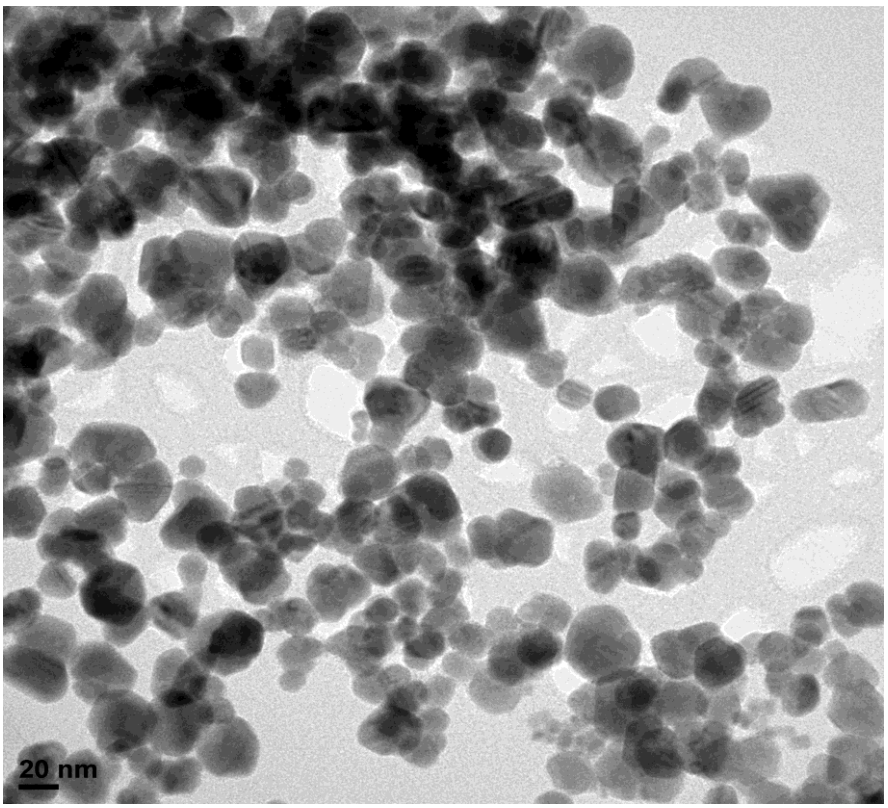

Figure 3.9a: TEM image of HgS nanoparticles at pH=4

As mentioned earlier, in aqueous media, the nanosized particles can be dispersed by the ionic repulsion forces generated due to different adsorbed species on their surface. This is evident here. These NPs remain well dispersed in solution for a long time. In aqueous solution, surfactants with cationic head groups control the synthesis of metal sulfide semiconductor NPs by binding S^{2-} ions [28].

Interestingly, the TEM imaging has proven the theory of Oswald ripening because *Wenling Jia et al* [36] found that with the addition of S^{2-}, the particle size of a ME^{x} (M being the metal, E^{x} being the chalcogenide) increases with the increase in sulphur [6]. What is relevant to this matter is that Nafion has a high concentration of sulphur, possibly disrupting the 1:1 ratio between Hg and S that was originally calculated. The addition of sulphur does not affect the number of already formed aggregates, it only alters their size. This may have been the reason in which the particles were slightly larger. However, the fact that the ionomer, Nafion was used meant that aggregates were not formed as shown in Figure 3.9a. It is likely that the use of this surfactant maintains a diffusion gradient using its permeability. The sample stayed colloidal as seen in Figure 3.9b.

Figure 3.9b: On the left is the solution containing pH=4 HgS with the addition of Nafion while the right contains HgS nanoparticles at pH=2 left for 24 hours

3.3. Cadmium and Bismuth

Preliminary experimentation was undertaken to witness the effects of thioacetamide on cadmium and bismuth. 300 µl of the thioacetamide solution was added into a vial containing 300 µl of cadmium solution. The results showed no instant colour change. However, after a short while, the solution changed colour and became slightly yellowish. It took roughly 8 minutes for this colour change to happen. The reason behind the rate of reaction and the rate of coagulation may lie in the structures of the precursors. Thioacetamide is a slow releasing substance which slowly releases sulphur, therefore limiting the rate of reaction. When this experiment was tried with bismuth instead of cadmium, the solution turned slightly peach in colour.

After initial tests to see if a colour change would occur when the two compounds were added, the actual concentrations based on the molecular weights of each metal and precursor were calculated. The thioacetamide caused a colour change which took around 10 minutes to become visible in both of the vials – one containing the cadmium solution and the other one bismuth.

Next, the preliminary testing for sodium sulfide as a precursor was prepared using a solution containing 1 gram of sodium sulfide and 1 litre of distilled water. 300 µl of sodium sulfide were added into a 300 µl vial of cadmium standard at 1000 ppm with 2% HNO_3. This produced an instant colour change to a deep yellow colour. However, after around 5 minutes coagulation had begun even under sonication. This experiment was repeated replacing cadmium with bismuth, which produced a colour change to a dark brown colour. The rate of reaction was significantly quicker than with the use of thioacetamide.

Similar to the preliminary testing with the thioacetamide, after these initial tests to see if a colour change would occur, the actual concentrations based on the molecular weights of each metal and precursor were calculated.

Sodium sulfide again showed instant colour change due to the rate of sulphur being released. Cadmium and bismuth, with the introduction of sodium sulfide looks very promising. However, coagulation had began to occur within a short period of time in both vials. Coagulation even occurred while the samples were in sonication baths. So it is evident that sodium sulfide is best suited for this reaction based on the quick rate of reaction.

3.3.1 Cadmium Sulfide

The addition of thioacetamide had shown a slow colour change, which took around 10 minutes. The solution had slowly turned a fluorescent green colour. The solution was transparent with a green tint to it. An EDX was carried out (Figure 3.10a). It confirms that CdS was synthesised and the copper shown as a peak represents the copper substrate the samples were placed on. After a day the colour was still present. No coalescing was visible. After 3 days coagulation was present and the solution had separated out. The particles became visible on the bottom of the vial. Within 3 days the fluorescent properties of the cadmium had began to slowly disappear. After 5 days the solution was clear. Figure 3.10b shows an SEM image of CdS with the use of thioacetamide.

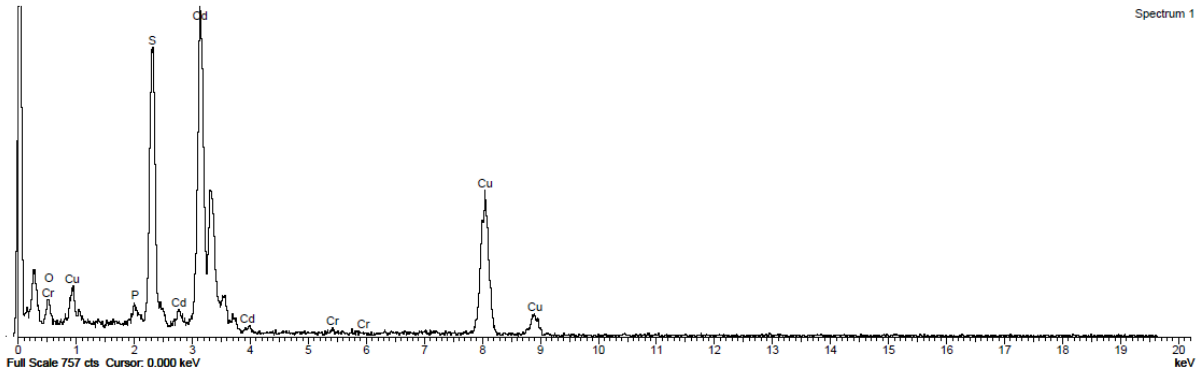

Figure 3.10a: EDX of CdS nanoparticles

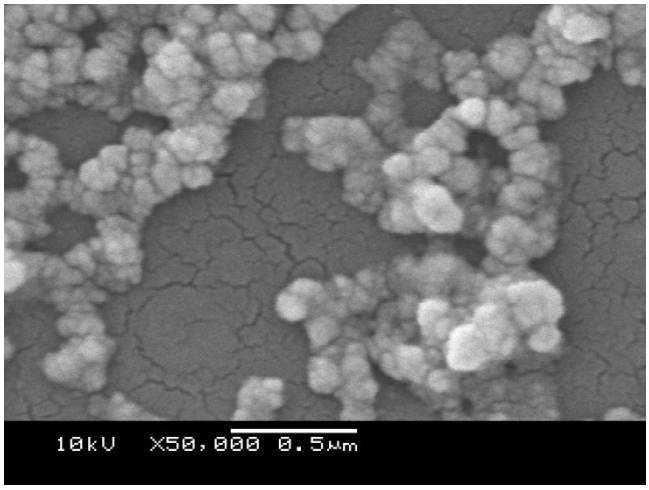

Figure 3.10b: SEM image of CdS using thioacetamide as the precursor

The use of sodium sulfide as a precursor for CdS nanoparticles showed a relatively quick colour change, with a reaction time around 30 seconds. The solution had turned a fluorescent green colour. The solution was again transparent with a green tint to it. After a day the colour was still present. Coagulation is apparent in Figure 3.10c and after 3 days full coagulation was present. The solution had separated out and the particles were visible on the bottom of the vial, with a clear liquid visible on top. Figure 3.10d shows TEM imagery of CdS with the addition of Nafion and what is obvious is that there are monodispersed nanoparticles present which are colloidal.

It must also be noted that during the 3 days the fluorescent properties of the cadmium had remained and after 5 days the solution had still retained its colour. Figure 3.10e shows the solution with the addition of Nafion after 5 days. Nafion is confirmed by the high fluorine peaks noticed on Figure 3.10f. It can be said that the addition of Nafion stabilised the particles and prevented them from both coagulation and photo-degradation, leaving them monodispersed. One might argue that the Ostwald ripening is present and has resulted in the decrease in the number of particles.

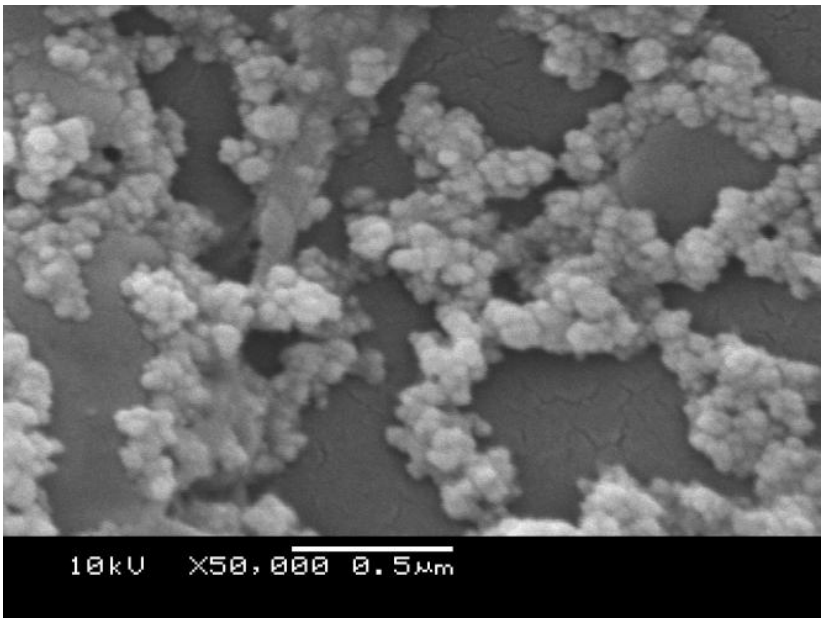

Figure 3.10c: SEM images of CdS using sodium sulfide as the precursor

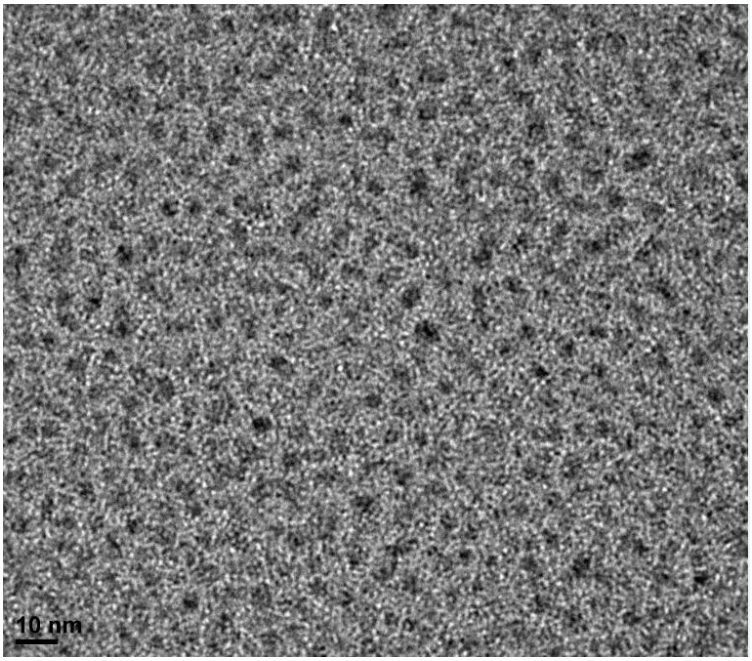

Figure 3.10d: TEM image of CdS using sodium sulfide as the precursor and with the addition of Nafion

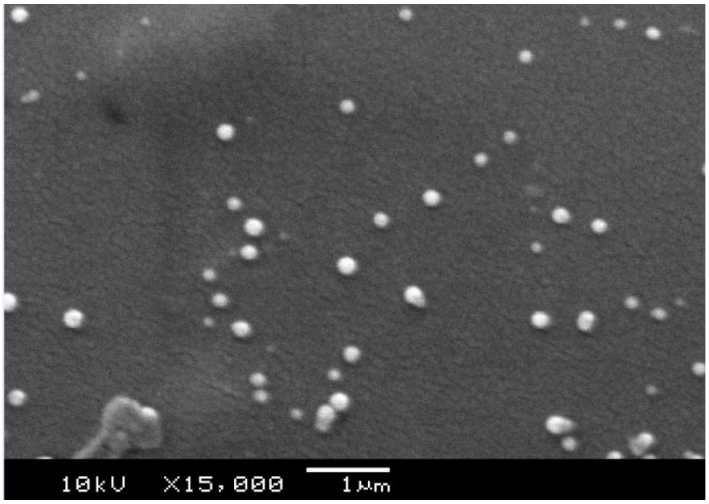

Figure 3.10e: SEM image which depicts CdS with the addition of Nafion

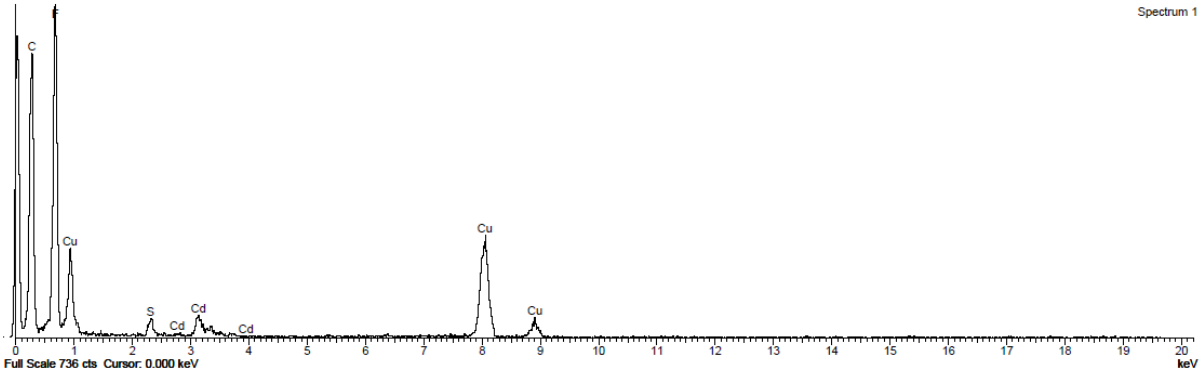

Figure 3.10f: EDX of CdS with the additive Nafion

3.3.2 Bismuth Sulfide

Despite bismuth with the sodium sulfide looking very promising, coagulation began within 2 minutes. Once again, the coagulation occurred while the sample was in the sonication bath. The sodium sulfide showed instant colour change. The bismuth sulfide was brown in colour yet had a glow to it, a brown fluorescent property. Once it had precipitated, large clumps of brown residue were visible at the bottom of the vial. Figure 3.11a shows heavy coagulation at the microscopic scale. Figure 3.11b shows the EDX for this solution and confirmation the bismuth sulfide nanoparticles were synthesised.

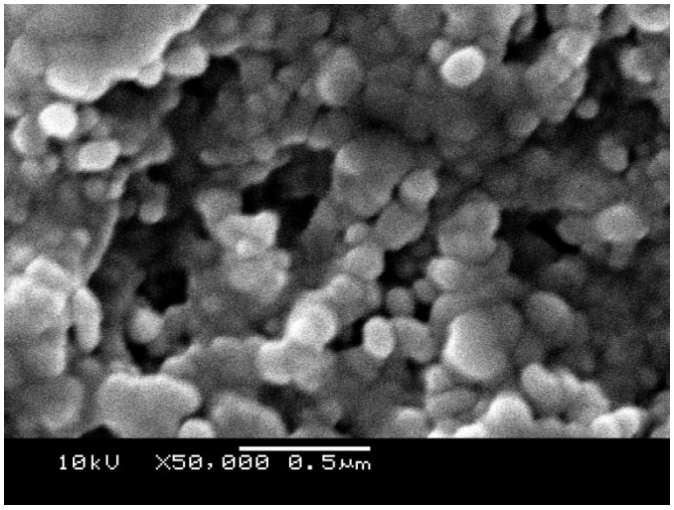

Figure 3.11a: SEM image showing clear signs of coagulation for the bismuth sulfide nanoparticles

The effect of thioacetamide upon the bismuth was very slow. It took around 10 minutes for a colour change to become visible. For thioacetamide the rate of coagulation was also slower. It took around 5 minutes for the coagulation to occur.

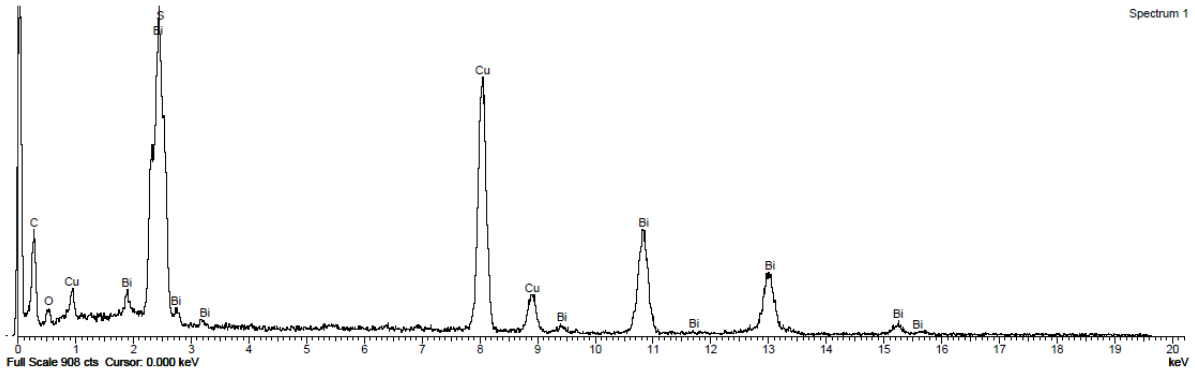

Figure 3.11b: EDX of bismuth sulfide nanoparticles

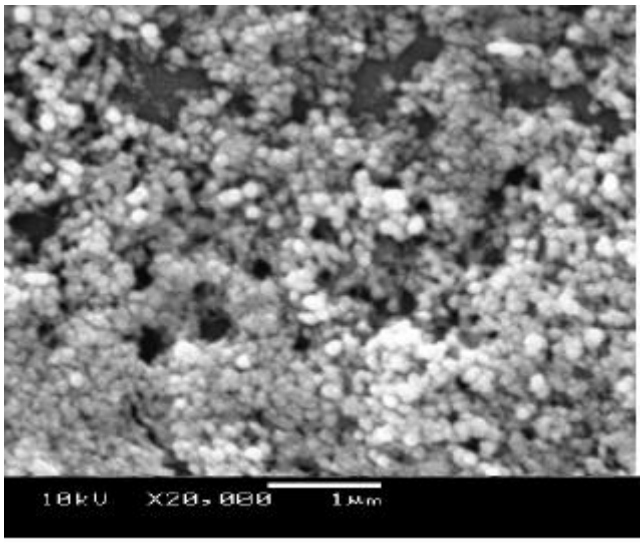

Figure 3.11c: SEM image of bismuth sulfide nanoparticles heavy coagulated

It is noticeable in Figure 3.11c that the thioacetamide was not optimum in the experiment. The sodium sulfide had increased the reaction time, quicker than that of thioacetamide, due to its quick release of sulphur. Thioacetamide was too slow in releasing its sulphur. This reason is not fully known. It may be due to the bonding sulphur has, and the parameters needed to break down these bonds. Schemes 4 and 5 show the formation of CdS and Bi_2S_3 respectively.

Scheme 4 representing the formation of CdS:

Scheme 5 representing the formation of Bi_2S_3

The addition of Nafion once again proved effective in the stabilisation of CdS and Bi_2S_3 nanoparticles using sodium sulfide. Figure 3.11d shows clear colloidal monodispersed bismuth sulfide nanoparticles. Figure 3.11e shows the EDX for bismuth sulfide nanoparticles with the addition of Nafion.

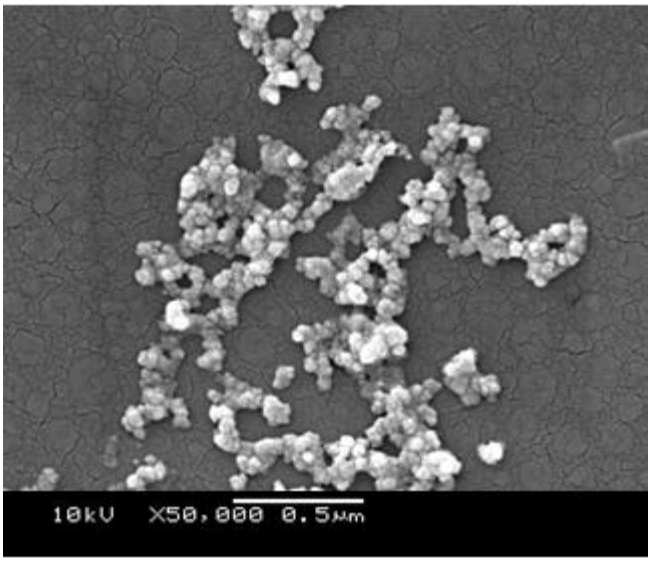

Figure 3.11d: SEM image of monodispersed bismuth sulfide nanoparticles with the addition of Nafion

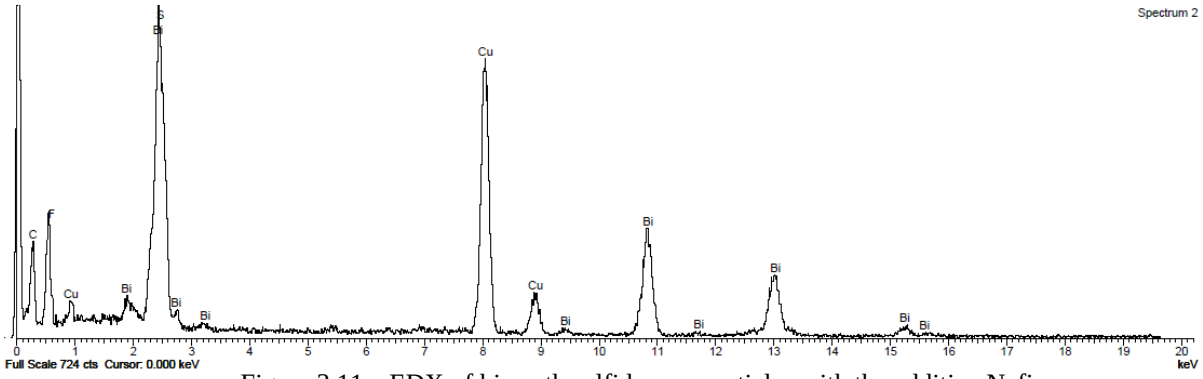

Figure 3.11e: EDX of bismuth sulfide nanoparticles with the additive Nafion

4. Conclusion

This thesis presents a novel methodology for producing mercury chalcogenides which has never been reported in this fashion. The nanoparticles growth is facile and fast producing, synthesising nanoparticles in the region of 8 to 20 nm (diameter). This is shown to be extendable to bismuth and cadmium which can improve an already established market in the field of nanotechnology. The effects of additives and solution composition have been explored and found to be critical to producing the desired chalcogenide nanoparticles. This thesis evaluated different possibilities in maintaining colloidal chalcogenide based nanoparticles after altering the solvent and a range of surfactants. The experiments brought to light have changed the current state of the arts in the synthesis and stabilising of HgS nanoparticles. This is due to the quick rate of reaction and the stability of the NPs formed. The size range of the nanoparticles is in line with previous literature but the main difference being the time taken for the particles to synthesise. It has been stated in this thesis that one of the key factors behind the rate of reaction is the optimisation in the nature to which the chalcogenide is introduced to the solution. The direct spiking of the precursor has been introduced to allow the particles to synthesise in a 1:1 basis with the metal solution. The controlling of the metal: precursor ratio is vital as this will alter the amount of Gibbs free energy; ultimately effecting the growth and nucleation of the nanoparticles. Understanding the fundamentals behind nucleation has led to different synthesis techniques which differ from the conventional top down assembly, as bottom up synthesis has been shown to have many advantages. Factors which could affect the nucleation rate and the size distribution have been looked at in order to maintain size distribution. These include diffusion, adsorption and the Ostwald ripening theory. Diffusion was controlled by the Nafion acting as a

membrane which allowed the movement of certain cations but not anions or electrons. This helped to maintain the metal: precursor ratio and ultimately kept PSD constant, resulting in monodispersed nanoparticles which do not coagulate. The most notable difference between the experiments presented here and that of previous literature is the increased speed of reaction. The time taken to synthesis the nanoparticles is substantially quicker. The overall stability of the mercury sulfide nanoparticles are of great importance as mercury is known to be a global contaminant of concern. This is due to its transformation by microorganisms to form methylmercury, a toxic species that accumulates in biological tissues. The low *Ksp* of mercury sulfide nanoparticles signifies its stability per mole, therefore being more stable and ultimately less harmful than naturally occurring mercury. The method of synthesis is also less harmful than those mentioned in previous literature i.e. milling/attrition.

The medicinal usage of nanoparticles has been a recent technological advancement. These advances include exploiting the small size and stable formation of the particles to use them as a core allowing siRNA to enter the body and into the relevant cells. Many biomedical experimentation have nanoparticles at the centre of their vectors when entering a host organism because a method of stability has been introduced and rapid facilitation of particles is available. The small size of the nanoparticles allows them to pass freely through the pores of the human eukaryotic membranes, preventing any unwanted build up of nanoparticles. The most common nanoparticle core used is gold due to its inactivity and inability to interfere with protein synthesis. There are no known reports of gold nanoparticles causing damage to the eukaryotic cell due to toxicity.

Appendix: siRNA applications in cancer research

Introduction

Recent research has been undertaken to bridge the gap between chemistry and the pharmaceutical realm. Nanoparticles are said to be the link between the two, exploiting their small nature and using their adjustable characteristics to benefit mankind. There have been many medicinal uses for nanoparticles such as cancer research, more specifically skin cancer. In order to understand skin cancer it is important to first understand the layers of skin which are affected. The top layer of the skin, the epidermis, is very thin and protects the deeper layers of skin and the organs. The bottom layer of the epidermis is made up of basal cells. These cells divide to form *keratinocytes*, which make a protein called keratin. This protein helps the skin protect the body.

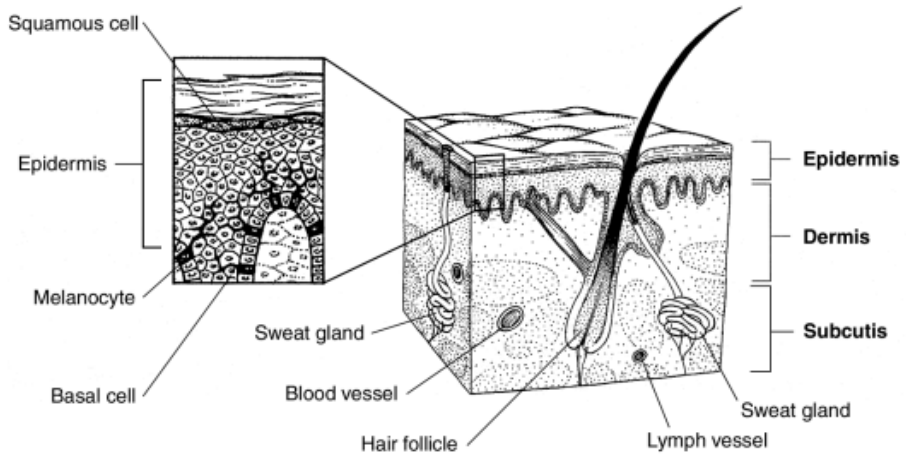

Figure A1: Diagrammatic cross section of the three layers of the skin [37]

The furthest out layer of the epidermis, the *stratum corneu*, is made up of dead keratinocytes that as newer cells are formed, are shed. The cells in this layer are called *squamous cells*. A cell type which is also found in the epidermis is the melanocyte. This is the cell responsible for making the brown pigment melanin. This is what gives the tan effect and the brown

colour which prevents the further layer from being affected by the harm which can be done by the sun. These cells are those that can become melanoma. The basement membrane, a layer which separates the epidermis from the deeper layers of skin, is important because when a skin cancer becomes more advanced it grows through this barrier. Melanoma is a cancer that begins in the melanocytes. The tumours often look black/brown due to the cells still forming melanin.

Transformation of normal melanocytes into melanoma cells is accomplished by the activation of growth stimulatory pathways, typically leading to cellular proliferation, and the inactivation of apoptotic and tumour suppressor pathways. A combination of genetic (somatic or hereditary) and epigenetic alterations is the basis for the instability characteristic of neoplastic transformation. Environmental insults, producing somatic mutations, are the most frequent abnormalities identified in human cancer. In melanocytic neoplasms, ultraviolet (UV) radiation from sunlight has been implicated as the primary environmental carcinogen [38].

A proto-oncogene is a normal gene that can become an oncogene due to mutations or increased expression. Oncogenes are genes which could potentially cause cancer. In tumour cells, they are often mutated or expressed at high levels. Usually cells undergo a regulated phase named apoptosis to regulate the amount of cells. Once the oncogenes are activated this can cause those cells that were due to die to survive and proliferate instead causing cancer. Proto-oncogenes may have many different functions in the cell. Some proto-oncogenes maintain apoptosis while others give signals that lead to cell division.

Oncogenes were first demonstrated in RNA tumour viruses, and further research revealed that they are derived from normal cellular genes called proto-oncogenes [39]. These proto-oncogenes have duties in cellular homeostasis, however, after the said alterations; it is known

that they become activated tumour-specific oncogenes. More than 70 oncogenes have been identified as participating in cellular proliferation, senescence, and apoptosis.

Oncogenes can cause a cell to divide in an unregulated manner. This growth can occur in the absence of normal growth signals such as those provided by growth factors. It must be known that a feature of oncogene activity is that a single changed copy can lead to unregulated growth.

Target genes implicated in cellular transformation and tumour progression have been divided into two categories. Activation of proto-oncogenes by point mutation, amplification, translocation, or even insertion of non-eukaryotic sequences, can produce oncogenes that have a 'gain' of function as their main characteristic. They have also been described as 'dominant' and 'positive' phenomena. Inactivation of tumour suppressor genes occurs mainly through an allelic deletion followed by a point mutation of the corresponding allele. These events have also been described as 'recessive' and 'negative'. Alterations in proto-oncogenes and tumour suppressor genes seem equally prevalent among human cancers. Specific genomic changes can yield different oncogenic effects [40]. Point mutations have the effect of altering the encoded proteins duty. Other point mutations, such as in the case of translocation, places an active promoter region or transcriptional regulatory element next to a proto-oncogene, causing the 'switch off' codon to potentially be shifted. This ultimately causes the oncogene to be continually expressed and proliferation to occur [41]. For example, the translocation for Burkitt lymphoma places the MYC gene under the control of the very active promoter for the heavy chain immunoglobulin cluster. Thus, the MYC protein is overproduced, and the cell proliferation genes are expressed.

As mentioned earlier, proto-oncogenes may be mutated to promote cell transformation by a variety of mechanisms: (a) point mutations may alter the function of the gene product and

produce a transforming protein (e.g. RAS and RAF in melanoma) and (b) translocations may activate the proto-oncogene (e.g. MYC).

Developments in research have highlighted both B-Raf and Akt3 as primary genes affected which cause melanoma. B-Raf, the most frequently mutated gene in melanoma, produces the mutant protein (proto oncogene B-Raf or v-Raf murine sarcoma viral oncogene homolog B1).

B-Raf helps mole cells survive and grow but does not form melanomas on its own. It has been previously found that a protein called Akt3 regulates the activity of the mutated B-Raf and aids the development of melanoma [44].

siRNA

siRNA (silencing ribonucleic acid or short interfering RNA) was first discovered by David Baulcombe's group at the Sainsbury laboratory in Norwich, England, as part of post-transcriptional gene silencing (PTGS) in plants. Shortly thereafter, in 2001, synthetic siRNAs were shown to be able to induce RNAi in mammalian cells by Thomas Tuschl, and colleagues in a paper published in *Nature* [45]. This discovery led to a surge in interest in harnessing RNAi for biomedical research and drug development.

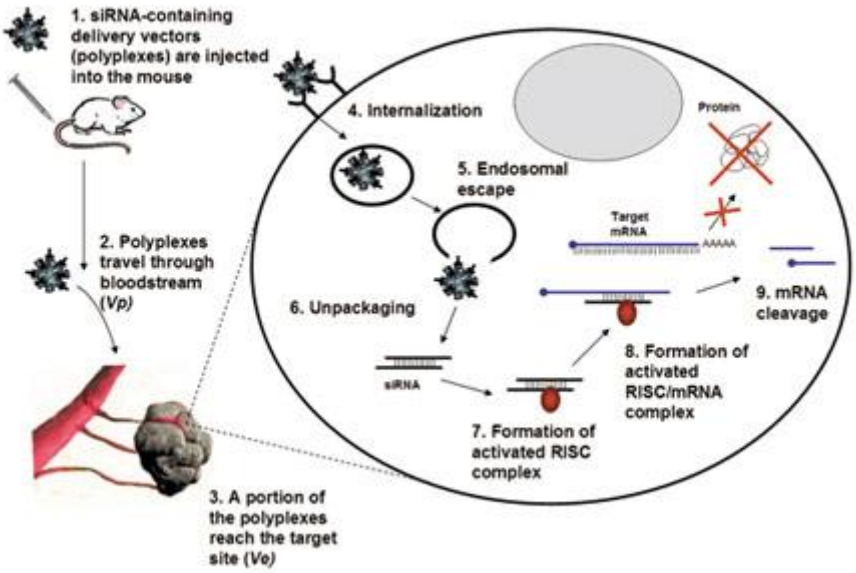

Figure A2*:* A diagrammatic representation of how siRNA works in mammals [42]

RNA-induced silencing complex, or RISC, is a multi-protein complex that incorporates one strand of siRNA. RISC uses the siRNA as a template for recognising complementary mRNA. When it finds a complementary strand, it activates RNase and cleaves the RNA.

The siRNA in this study specifically targets Akt3 and the mutant B-Raf and does not therefore affect normal cells. The theory behind the concept is siRNA would knock out specific genes i.e. suppress gene expression potentially turning off the two cancer causing genes and effectively treating the disease.

Mice with melanoma that underwent the same treatment had their tumours shrink by nearly 30 percent when only the mutant B-Raf was targeted. There was no difference in the development of melanoma when the Akt3 gene alone was targeted, though existing tumours shrank by about 10 to 15 percent in two weeks. However, when the researchers targeted both

the Akt3 and the mutant B-Raf at the same time, they found that tumours in the mice shrank by about 60 to 70 percent more than when either gene was targeted alone [43].

However there are downsides to this treatment. A quote from Gavin Robertson revealed "If you knock down each of these two genes separately, you are able to reduce tumour development somewhat". Robertson went on to say "but knocking them down together leads to synergistic reduction of tumour development protective layers in the skin not only keeps drugs out, but chemicals in the skin quickly degrade the siRNA [47].

This was a huge hurdle in the progress of the elimination of cancer. The research group decided to synthesise hollow nanosized particles called nanoliposomes, from globes of fatty acids into which they packed the siRNA. They used an ultrasound device to temporarily create microscopic holes in the surface of the skin, to allow the particle to leak into tumour cells beneath [46].

Experiment

The interaction with the cell membranes is very important for these delivery systems. This represents the most important aspect in gene delivery. The pathway for cellular entry can determine if the nucleic acid is transported to its expected site and also controls its effectiveness. A method proposed by *Elbakry et al* [44] involved the use of gold nanoparticles which has recently proved most effective. This experiment is at the pinnacle of research in cancer as this has shown the most promise in the suppression of tumours and is the closest to succeed in the fight against cancer. The principles introduced in this experiment are well structured, as the siRNA is forced inside the body via a synthetic vector made with a nanoparticle core. The solid and stable properties of gold nanoparticles were the underlining factor behind this particular method. Gold nanoparticles were synthesised using the *Turkevich*

method. The synthesised nanoparticles were then coated in MUA (11-Mercaptoundecanoic Acid) then centrifuged as it is a known surfactant for gold nanoparticles, shown by the work of *Hoon Kim et al* [35]. 16-Mercaptohexadecanoic acid 99% and polyethyleneimine branched were purchased from Sigma Aldrich. Strains of siRNA were purchased from Qiagen and Figure A3 illustrates the experimental method.

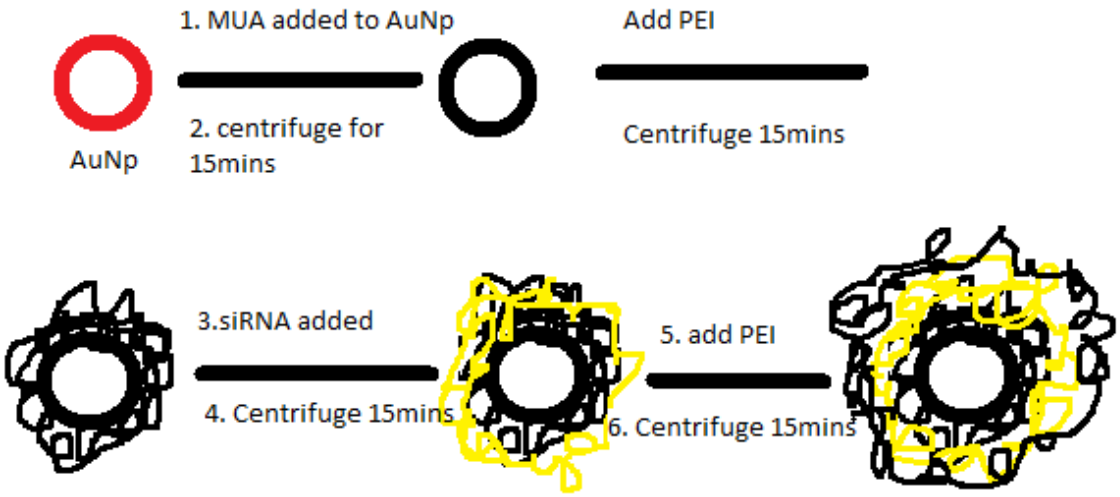

Figure A3: A step by step methodology of the process of synthesising gold based siRNA complex

Next it was vital to initiate the first layer of the complex. This was the well known polymer poly(ethyleneimine) (PEI). However it was important to balance the ionic strength as random self assembled aggregates of PEI and nucleic acid may suffer from severe aggregation when subjected to high ionic strengths of biological fluids. The sample was then centrifuged and siRNA was added. After centrifuging the samples the final layer of the PEI was added. This is depicted in Figure A3. In the development of gene technology, it is vital to fully understand state of the art techniques in order to progress. The goal here is to recreate and gain a deeper understanding of this experiment in order to identify any weaknesses in the method and to

then be able to progress. The ultimate aim is to strengthen any flawed areas this experiment contains and then build upon these to create the perfect method of gene transfer and suppression.

UV-Vis of the samples at each coating stage showed the growth of the complex as seen in Figure A4. SEM imagery confirms this in Figures A5, A6 and A7.

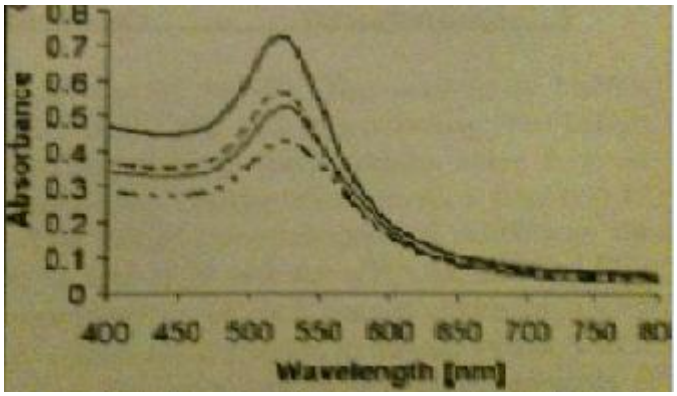

Figure A4: UV-Vis spectra after each coating stage

The figures read AuNps 525 nm being the highest visible peak, PEI-AuNps, 529 nm; siRNA-PEI-AuNps, 533 nm; PEI-siRNA-PEI-AuNps, 537 nm being the lowest visible peak. The change in the figures at each coating stage could be a result of adsorption of proteins on the surface. Figure A6 shows gold nanoparticles as the core of the experiment.

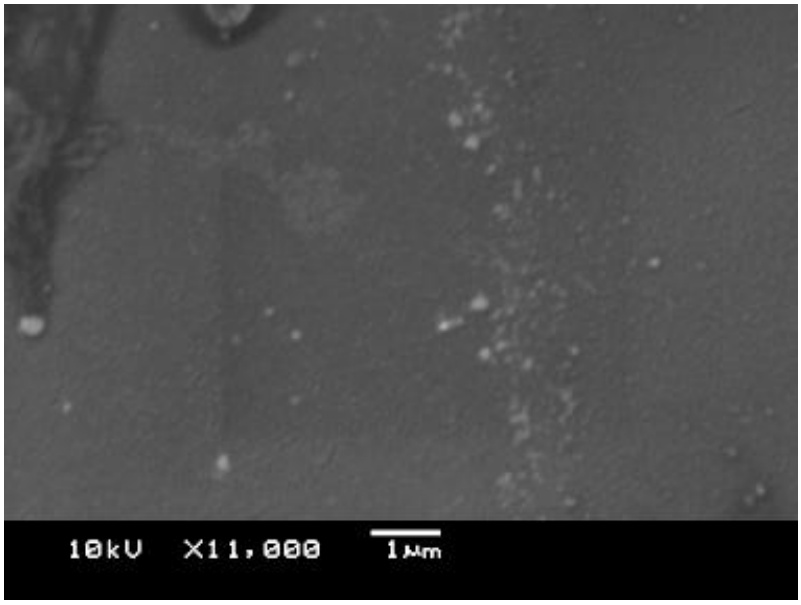

Figure A5: SEM image of gold nanoparticles without the addition of any additives

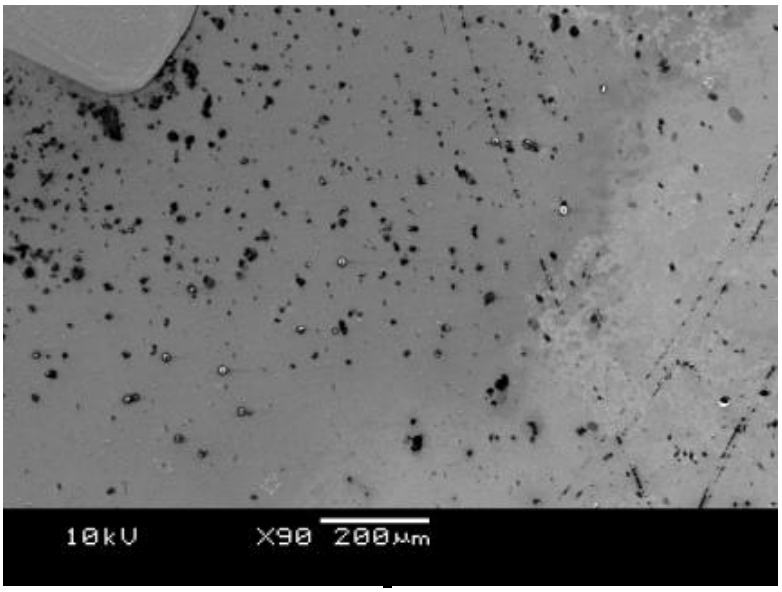

Figure A6: SEM image of gold nanoparticles coated in MUA

Figure A5 shows a distant view of the gold nanoparticles once synthesised, while Figure A6 is a depiction of the same gold nanoparticles once coated in MUA.

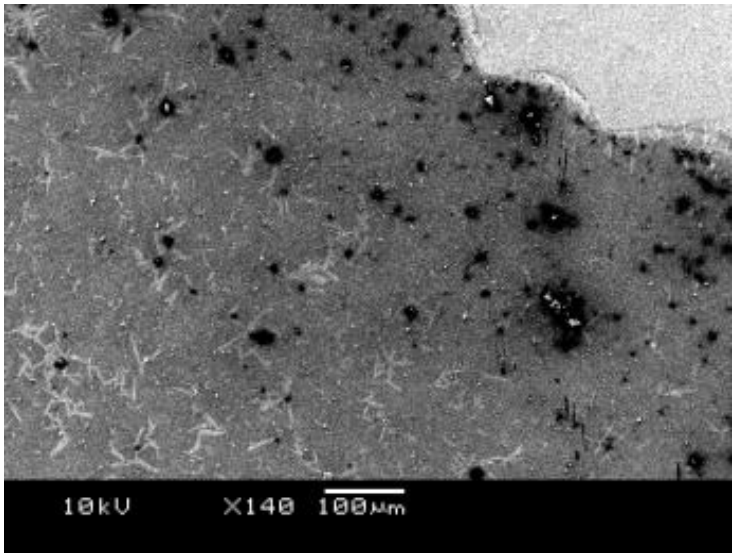

Figure A7: SEM image of the coated gold nanoparticles in a PEI suspension

Figure A7 shows the coated nanoparticles in a suspension which is the PEI. The whole structures are the long polymer chains of PEI.

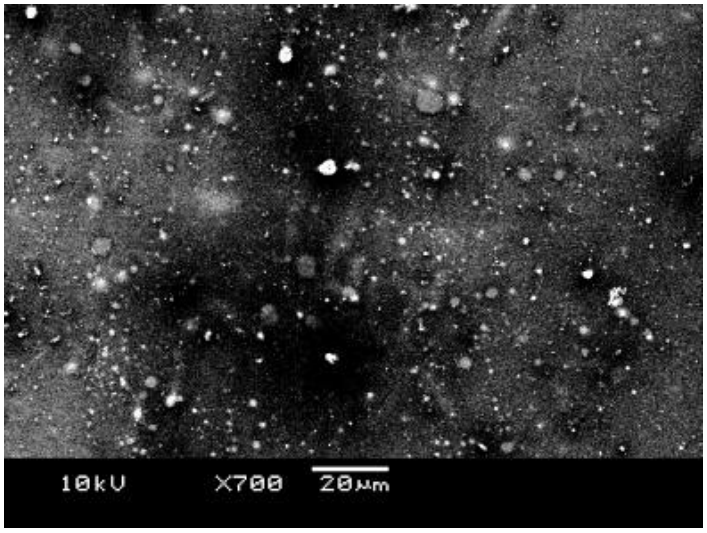

Figure A8: SEM image of the coated gold nanoparticles encompassed in PEI

Although Figure A7 showed structures of PEI, Figure A8 is an in detail examination of these same structures. What must be noted is the concentration of the gold nanoparticles held tangent within these structures. Figures A9 and A10 show what the cluster looks like once

siRNA is added. It is interesting to see, there seems to be a capsule like structure. These images were not seen before in the initial research. Figure A11 shows the final structure after the last layer of PEI is added. It looks as if clusters are formed encapsulating the siRNA.

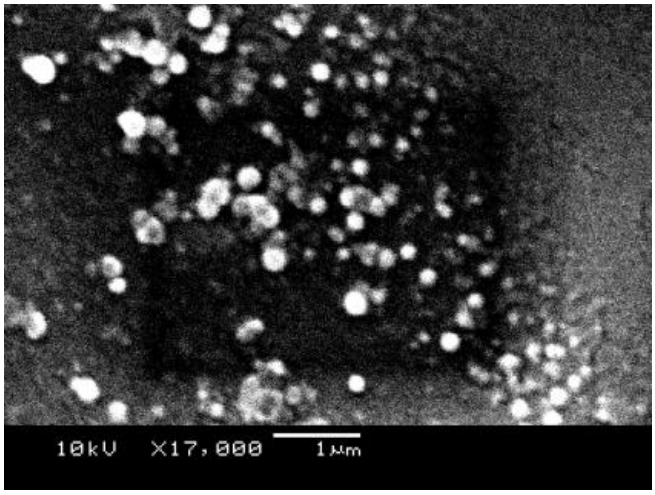

Figure A9: SEM image of siRNA when introduced in the clusters

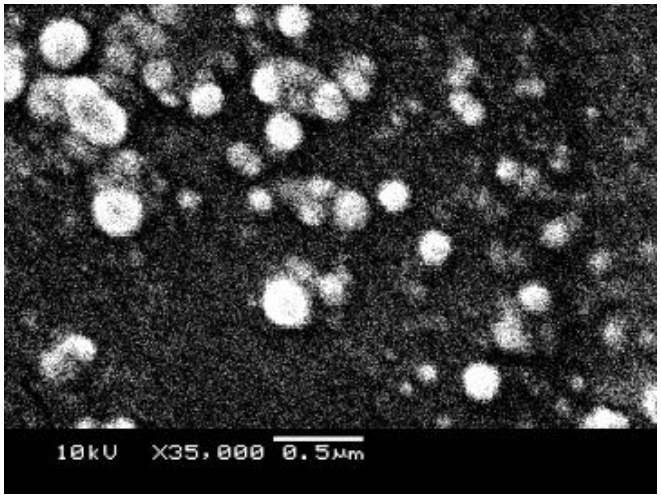

Figure A10: SEM image at higher magnification of the siRNA once introduced into the clusters

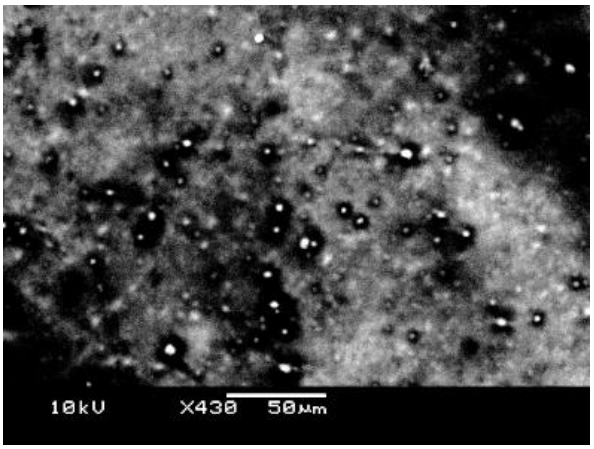

Figure A11: SEM image of the final layer by layer cluster once the final layer of PEI was added

Despite successfully introducing the siRNA into the complex, the next task was to insert the complex into eukaryotic cells. However this had its downside. The eukaryotic cells saw this vector as a foreign body and endocytotic organelle engulfed it. After 6 hours of incubation no siRNA was detected within the nucleus. What was remarkable was that despite being inside the endocytotic organelle, the structure remained intact. This inspires hope for the next generation of experiments. Those involved in this experiment predicted that a biodegradable polymer is needed for the outer coat for sufficient release inside the body. Another recommendation would be to attach an antigen to protect the cluster from endocytotic organelle. These organelle would recognise the antigen and would ultimately stop the cluster from being engulfed.

Further Experimentation

The biological applications of siRNA seem to be progressing at a rapid rate. It is very likely that the suppression of cancer could be achieved within the decade. The problem of finding a suitable vector for inserting the siRNA into the human body is likely to be found shortly. Due to my time constraints I was not able to advance in my experiments. My next idea was to attach a suitable antigen to the cluster in order to prevent any endocyte from engulfing the cluster. To overcome the problem of the outer shell not being degraded I would have used a form of starch coat as the outer layer. So once inside the body, specific enzymes would have broken down the coat releasing the wanted content. My next alteration would have been to use iron oxide as the central nanoparticle. This is due to the magnetic properties of iron. This could have been exploited in manoeuvring the structure to the desired location capitalising on these magnetic properties. My final alteration would have been attaching a marker upon the cluster in order to monitor its location with a fluorescent dye, which can be monitored within the body.

5. References

[1] B. Cowin, *Scientific Committee on Emerging and Newly Identified Health Risk,* 2006, **3**, 6

[2] B. O. Dabbousi, M.G. Bawendi, O. Onitsuka, and M. F. Rubner, *Appl. Phys. Lett.*, 1995, **66**, 1361

[3] F.A. Ababneh, S.L. Scott, A.L. Reasi and H.A. Lean, *Sci. Total Environ.*, 2006, **367**, 831

[4]W. M. Zhiming, *J. Am. Chem.*, 2008, **92**, 250

[5] M. Hauta and B.D.R. Elmon, *J. Phys. Chem.*, 1986, **80**, 859

[6] D. V.Goia, *J. Matt. Chem.*, 2004, **2**, 4

[7]M. Elimelech, M. Borkovec and J. Hering, *Appl. Phys. Lett.*, 1999, **239**, 316

[8] L. E. Berre and I.C. Sadron, *Chem. Rev.*, 1997, **112,** 312

[9] S. V. Gapoenko, *Cambridge University Press*, 2003, **45**, 4

[10] V. L. Colvin, M. C. Schlamp and A. P. Alivisators, *Nature.*, 1994, **355,** 354

[11] C. K. Gratzel and A. Gratzel, *J. Am. Chem.*, 1979, **67,** 7741

[12] A. Hangfeldt and M. Gratzel, *Chem. Rev.*, 1995, **95**, 49

[13] T. Pradeep, *J. Phys. Chem.*, 2007, **385,** 5

[14]P. Padhi, G. Sahoo, K. Das, S. Ghosh and S. C. Panigrahi, *Nanoscopic and Macroscopic Materials,* 2008, **63,** 431

[15] K. Zhang, T. Kim, B. Levard, C. Reinsch, B. C Lowry and G V. Deshusses, *ACS Publications*, 2012, **3**, 23

[16] PH. Xu and T. Ling, *J. Am. Chem*., 2003, **136,** 2741

[17]A. K Mahapatra and A.K. Dash, *Physica. E.*, 2006, **44,** 125

[18] B.K. Patel, S. Rath and S. Sarangi, *Materials Science & Processing*, 2007, **86**, 447

[19] Q. Nie, Q. Yuan and W. Chen, *J. Cryst. Growth*, 2004, **265**, 420

[20] X. Ma, F. Xu and Z. Zhang, *Mater. Res. Bull*., 2005, **40**, 2180

[21] Y. Wang, C.Y. Ho and D.H. Ning, *Mater. Lett.,* 2006, **66**, 1151

[22] R. Romano and O. L. Alves, *Mater. Res. Bull.,* 2006, **47**, 376

[23] Y. Yang, H. Chen and X. Bao, *J. Cryst. Growth*, 2003, **252,** 251

[24] A. Dumbrava, C. Badea and G. Prodan, *Chalcogenide Letters*, 2010, **7,** 111

[25] P.R. Gogate and A.B. Pandit, *Adv. Environ. Res*., 2004, **8**, 501

[26] R. Yuan, R. Guan, W. Shen and J. Zheng, *Colloid. Interface Sci.,* 2005, **282**, 87

[27] N. Dubey, S.S. Rayalu, N.K. Labhsetwar and S. Devotta, *Int. J. Hydrogen Energy*, 2008, **33,** 5958

[28] S. Murray and C. Hammond, *Mater. Res. Bull*., 2009, **75,** 89

[29] Nanotechnology Emerging Technologies, www.nanowerk.com/news/newsid=20107.php, (accessed September 2011).

[30]Y. Zhao, *Mater. Lett*., 2004, **58**, 790

[31]F. X.Han, Y.Su, D. L. Monts and Y. Xia, *World Congress of Soil Science*, 2010, **1**, 1

[32] J.P. Han, S. Shiyab, T. Tsung, R.J. Taylor and C.A. Waggoner, *Mater. Lett*., 2007, **76**, 167

[33] K.Y. Hoon, *Chem. Letters*, 2004, **3**, 344

[34] L. M. Mansfield, I. L. Repins and S. Glynn, *Mater. Lett*., 2011, **3,** 56

[35] S. Lee, T. L. Yu, A.B. Hsiu-li, A.B. Lin and W.H. Liu, *Mater. Lett.,* 2004, **45**, 2853

[36] J. Wenling and E.P. Douglas, *J. Am. Chem*., 2003, **14**, 744

[37] L. Rosen and G. Rosen, *American Cancer Society*, 2011, **1**, 278

[38] D. Polsky and C. Cordon, *Nature*., 2003, **425**, 3087

[39] H. G. Vamus, *Cancer.,* 1985, **32**, 2324

[40] C. J. Tabin, S.M. Bradley and C.I. Bargmann, *Nature.,* 2002, **300**, 43

[41] S. V. Hodgson and E. R. Maher, C*ambridge Press*, 1997, **29**, 95

[42] Melanoma and Akt3 in Mammalian Cells, http://www.medgadget.com/oncology/page/4, (accessed September 2011)

[43] Mutation of B-raf, http://www.sciencedaily.com/releases/2012/04/120404102646.htm, (accessed September 2011)

[44] A. Elbarky, A. Zaky, R. Liebi and R. Rachel, *Nano. Lett.*, 2009, **9**, 235